

# Klein-Nishina Effects in the Spectra of Non-Thermal Sources Immersed in External Radiation Fields

Rafał Moderski <sup>1</sup>, Marek Sikora <sup>1</sup>, Paolo S. Coppi <sup>2,3</sup>, and Felix Aharonian <sup>3</sup>

## ABSTRACT

We provide a systematic numerical and analytical study of Klein-Nishina (KN) effects in the spectrum produced by a steady state, non-thermal source where rapidly accelerated electrons cool by emitting synchrotron radiation and Compton upscattering ambient photons produced outside the source. We focus on the case where  $q$ , the ratio of the ambient radiation field to source magnetic field energy densities, significantly exceeds unity. We show that the KN reduction in the electron Compton cooling rate causes the steady-state electron spectrum to harden at energies  $\gamma \gtrsim \gamma_{KN}$ , where  $\gamma_{KN} = 1/4\epsilon_0$  and  $\epsilon_0 = h\nu_0/m_e c^2$  is the characteristic ambient photon energy. This hardening becomes noticeable in the synchrotron radiation from electrons with energies as low as  $0.1\gamma_{KN}$  and changes the synchrotron spectral index relative to its Thomson limit value by as much as  $\Delta\alpha \sim 0.75$  for  $q \gg 1$ . The source synchrotron spectrum thus shows a high-energy “bump” or excess even though the electron acceleration spectrum has no such excess. In contrast, the low-energy Compton gamma-ray spectrum shows little distortion because the electron hardening compensates for the KN decline in the scattering rate. For sufficiently high electron energies, however, Compton cooling becomes so inefficient that synchrotron cooling dominates – an effect omitted in most previous studies. The hardening of the electron distribution thus stops, leading to a rapid decline in Compton gamma-ray emission, i.e., a strong spectral break whose location does not depend on the maximum electron energy. This break can limit the importance of Compton gamma-ray pair production on ambient photons and implies that a source’s synchrotron luminosity may exceed its Compton luminosity even though  $q > 1$ . We discuss the importance of these KN effects in blazars, micro-quasars, and pulsar binaries.

*Subject headings:* quasars: jets — radiation mechanisms: non-thermal — MHD

---

<sup>1</sup>Nicolaus Copernicus Astronomical Center, Bartycka 18, 00-716 Warsaw, Poland; moderski@camk.edu.pl

<sup>2</sup>Yale University, New Haven, CT 06520-8101, USA

<sup>3</sup>Max-Planck-Institut für Kernphysik, Heidelberg, Germany

## 1. INTRODUCTION

Probably because of the initially greater sensitivity of radio telescopes, studies of the emission from non-thermal sources, e.g., the powerful radio jets found in AGN, focused on synchrotron radiation from relativistic electrons moving in a magnetic field. It was quickly realized, however, that the same relativistic electrons would also Compton upscatter any ambient low-energy photons to produce emission at much higher, e.g., X-ray and gamma-ray, energies. A classic discussion of the emission spectrum expected from a gas of relativistic electrons where synchrotron radiation and Compton scattering are the dominant energy loss mechanisms may be found, for example, in Felten & Morrison (1966). Several of the standard approximations still used today are presented there, e.g., the delta function approximation which provides a one-to-one relation between the energies of the electrons and the synchrotron and Compton upscattered photons produced by them. Of particular interest, those authors note that the processes of Compton upscattering in the Thomson regime and synchrotron radiation both lead to quasi-continuous electron energy losses that are proportional to the square of the electron Lorentz factor. (This is in fact not a surprise given that synchrotron radiation may be viewed as the Compton upscattering of virtual magnetic field photons [see Blumenthal & Gould 1970].) This implies that the shape of the energy distribution of cooled electrons does not depend on which process dominates their cooling and that the ratio of the luminosities for the resulting Compton and synchrotron emission components simply goes as  $L_C/L_{syn} = u_0/u_B$ , where  $u_0$  and  $u_B$  are respectively the (co-moving) low-energy radiation and magnetic field energy densities inside the source. This is very useful to know, for example, since if one measures  $L_C$  and  $L_{syn}$  and knows  $u_0$ , e.g., if the relevant low-energy ambient photons are due to the cosmic microwave background, then one can immediately derive the magnetic field strength in the source. Also, the shapes of the synchrotron and Compton emission spectra will be similar, with the Compton spectrum simply shifted up in energy relative to the synchrotron one by the factor  $\epsilon_0/\epsilon_B$  where  $\epsilon_B = B/B_{cr}$ ,  $B_{cr} = 4.4 \times 10^{13}$  G, and  $\epsilon_0 = h\nu_0/m_e c^2$  is the typical ambient photon energy. (For mono-energetic ambient photons, the spectral shapes are in fact identical except for the effects of self-absorption in the low-energy portion of the synchrotron spectrum.)

It is important to remember, however, that all of these convenient rules of thumb, used in many interpretation papers, break down when the electrons are sufficiently energetic to scatter with ambient photons in the Klein-Nishina (KN) limit, i.e., when  $\gamma > \gamma_{KN} = 1/4\epsilon_0$  (e.g., Blumenthal & Gould 1970). In this case, the relation between upscattered and incident photon energy changes (the upscattered photon cannot have more energy than the incident electron), electrons can lose most of their energy in a single scattering rather than cooling quasi-continuously as a result of many small energy losses, and to the extent that a cooling rate is relevant, the ratio of Compton to synchrotron energy losses is now a decreasing

function of energy and is less than  $u_0/u_B$ . A careful re-examination of the implications of treating the Compton scattering process correctly in this limit is timely now that satellite and ground-based gamma-ray telescopes have shown many extragalactic and some galactic compact objects to be strong emitters of GeV and TeV radiation. If produced by Compton up-scattering, i.e., the Inverse Compton (IC) process, then these gamma-rays likely result from scatterings in the KN regime, and we must be accordingly careful in the interpretation of the multi-wavelength observations for these objects.

Some of the possible KN “corrections” have already been discussed or are well-known. An obvious limit is the case when the ambient (target) photon energy density in the source is small and the energy density ratio  $q = u_0/u_B$  is thus  $\ll 1$ . In this case, synchrotron losses always dominate over Compton losses regardless of electron energy. If we have a source where electrons are rapidly accelerated to high energies and subsequently cool via radiative losses, then the steady state spectrum of the source (assuming on-going acceleration) is determined solely by the magnetic field and the “injection” energy spectrum of electrons produced by the rapid acceleration process. We can therefore consider the electron distribution to be fixed, e.g., a power law with  $n_\gamma \propto \gamma^{-s}$ , and just need to carry out the relatively easy computation of the Compton spectrum upscattered by such an electron power law. For simplicity, let us assume that the ambient radiation field is approximately mono-energetic, again with characteristic energy  $\epsilon_0$ . In this case, the resulting Compton emissivity is approximately a broken power law, with the usual Thomson-limit result of  $j_\epsilon \propto \epsilon^{-(s-1)/2}$  for  $\epsilon \ll \epsilon_{KN}$ , and the extreme KN-limit result of  $j_\epsilon \propto \epsilon^{-s} \log(\epsilon)$  for  $\epsilon \gg \epsilon_{KN}$  where  $\epsilon_{KN} = \gamma_{KN}$ , e.g., see Aharonian & Atoyan (1981). In other words, the synchrotron spectrum is unchanged from a Thomson-approximation calculation while the Compton spectrum shows a strong spectral break at  $\epsilon \sim \epsilon_{KN}$  with a change in spectral index  $\Delta\alpha = (s + 1)/2$ . For  $s \gtrsim 2$ , which seems typical for the known very high-energy gamma-ray sources,  $\Delta\alpha \gtrsim 1.5$ , i.e., is large, and given the usually poor statistics at the highest energies, this spectral break can easily be misinterpreted as a an exponential cutoff due to the maximum electron energy in the source.

A much less obvious but still important limit is the case  $q \gg 1$ . For  $u_0$  sufficiently large, one can in principle go the opposite limit and ignore the effects of synchrotron cooling, solving directly the kinetic equation for the evolution of electrons due to Compton scattering. The steady state electron and upscattered photon spectra obtained for continuous electron acceleration and complete electron cooling via Compton scattering are discussed in detail by Zdziarski (1989) (see also Zdziarski & Krolik, 1993). The main conclusion is that the equilibrium electron distribution hardens for  $\gamma > \gamma_{KN}$  compared to the Thomson approximation result. This is because electron energy losses are relatively less efficient in the KN limit and electrons remain longer at higher energies. This hardening of the electron spectrum compensates the decreased efficiency of Compton upscattering, and the resulting photon spectrum

shows *no* “Klein-Nishina break” at  $\epsilon \sim \epsilon_{IC,KN}$ . Interestingly, for a rapid acceleration process that effectively injects electrons into the source with an energy distribution  $Q(\gamma) \propto \gamma^{-p}$  with  $p = 2$ , the Compton emissivity is  $j_\epsilon \propto \epsilon^{-2}$ , i.e., exactly the answer that would have been obtained in the Thomson limit. Note, though, an important difference from the Thomson result is that the correctly computed spectrum always cuts off at  $\epsilon \sim \gamma_{max}$ , the maximum electron Lorentz factor, and that this cutoff is independent of the target photon energy  $\epsilon_0$ . Also, for  $p \neq 2$ , the Compton spectrum in the KN regime does not follow the slope of the spectrum in the Thomson regime, steepening a bit if  $p > 2$ , and hardening if  $p < 2$ .

The analysis just mentioned, however, do not include synchrotron losses and do not consider the synchrotron emission produced as a result of these losses. (The condition  $q \gg 1$ , in fact only guarantees that synchrotron losses are negligible for  $\gamma < \gamma_{KN}$ . At higher energies, the Compton loss rate decreases due to KN effects and eventually synchrotron cooling always dominates.) They thus miss several effects that are potentially important for high energy sources. First, the hardening of electron distribution in the KN regime leads to a hardening of co-spatially produced synchrotron radiation. Prior work which touches on this aspect includes: Dermer & Atoyan (2002) which invokes KN effects to help explain the production of X-rays in large scale jets via synchrotron radiation; Ravasio et al. (2003) which invoke KN effects to explain the spectral “glitch;” Kusunose, Takahara & Kato (2004) and Kusunose & Takahara (2005) which study KN effects in the context of FSRQ (flat-spectrum-radio-quasars). Secondly, for sufficiently high electron energies, synchrotron losses dominate and the electron distribution “saturates” to one with the same slope as in the Thomson regime, but with a normalization factor  $q$  times larger. This effect was included by Khangulian & Aharonian (2005) in their studies of outflows from compact objects in high mass X-ray binary systems, but not by Kusunose & Takahara (2005), even though some of their calculations involve electron energies high enough for synchrotron losses to be important.

In this paper, we provide a systematic study of KN effects in steady-state sources with  $q \gg 1$ , covering all the effects mentioned above. We use accurate numerical techniques that solve the exact integro-differential equations for the steady-state photon and electron energy distributions. However, we also present approximations that allow one to follow the various effects analytically using simple algebraic functions. We focus our studies on the case where the ambient radiation field is dominated by external photon sources with mono-energetic or power-law spectra. The paper is organized as follows. In §2 we analyze inverse-Compton electron energy losses in the KN regime and compare them with the corresponding synchrotron energy losses. In §3 we present general and approximate formulas for the inverse-Compton emissivities for the cases of isotropic and beamed ambient radiation fields. The energy distribution of relativistic electrons in a steady-state source with continuous electron injection is discussed in §4. The KN effects in the synchrotron and inverse-Compton spectra

produced by such a source are analyzed in §5. Our results are discussed in the context of specific astrophysical sources in §6 and summarized in §7.

## 2. ELECTRON ENERGY LOSSES

### 2.1. Inverse Compton energy losses

The rate of inverse Compton (IC) energy losses of relativistic, isotropically distributed electrons is (see Appendix A)

$$|\dot{\gamma}|_{IC} = \frac{4c\sigma_T}{3m_e c^2} u_0 \gamma^2 F_{KN}, \quad (1)$$

where

$$F_{KN} = \frac{1}{u_0} \int_{\epsilon_{0,min}}^{\epsilon_{0,max}} f_{KN}(\tilde{b}) u_{\epsilon_0} d\epsilon_0, \quad (2)$$

$u_0 = \int_{\epsilon_{0,min}}^{\epsilon_{0,max}} u_{\epsilon_0} d\epsilon_0$  is the total energy density of the radiation field,  $u_{\epsilon_0}$  is the energy distribution of the ambient photons, and we re-express the electron energy as  $\tilde{b} = 4\gamma\epsilon_0$  noting  $\tilde{b} = 1$  corresponds to the transition between the Thomson and KN scattering regimes. The function  $f_{KN}(\tilde{b})$  is given by Eqs. (A12) and (A10) in Appendix A. For  $\tilde{b} \ll 1$  (Thomson limit),  $f_{KN} \simeq 1$ ; for  $\tilde{b} \gg 1$  (KN limit),  $f_{KN} \simeq (9/(2\tilde{b}^2))(\ln \tilde{b} - 11/6)$ . For  $b \lesssim 10^4$ ,  $f_{KN}(\tilde{b})$  can be approximated by

$$f_{KN} \simeq \frac{1}{(1 + \tilde{b})^{1.5}}. \quad (3)$$

To estimate the effects of having an extended target photon energy distribution, let us assume that  $u_{\epsilon_0}$  is a power law  $\propto \epsilon_0^{-\alpha}$  and that  $b_{max} = 4\epsilon_{0,max}\gamma_{max} < 10^4$ , so we may use approximation (3). Then we may write,

$$F_{KN} \propto \int_{\epsilon_{0,min}}^{\epsilon_{0,KN}} \epsilon_0^{-\alpha_0} d\epsilon_0 + \epsilon_{0,KN}^{1.5} \int_{\epsilon_{0,KN}}^{\epsilon_{0,max}} \epsilon_0^{-\alpha_0-1.5} d\epsilon_0, \quad (4)$$

where  $\epsilon_{0,KN} = 1/4\gamma$ . KN effects become important and  $F_{KN} < 1$  for  $\gamma > \gamma_{KN} \equiv 1/(4\epsilon_{0,max})$ . For  $\alpha_0 < -0.5$ , Compton energy losses for electrons with  $\gamma > \gamma_{KN}$  are dominated by scatterings on photons with the highest energies,  $\sim \epsilon_{0,max}$ . We may then treat the photon distribution as mono-energetic, with  $F_{KN} \simeq f_{KN}(\tilde{b} = 4\gamma\epsilon_{0,max})$ . For  $-0.5 < \alpha_0 < 1$ , Compton losses are instead dominated by scattering on photons with energy  $\sim \epsilon_{0,KN}$ . In this case, we may make the so-called ‘‘Thomson-edge’’ or ‘‘Klein-Nishina cutoff’’ approximation that

$$F_{KN} \simeq \frac{\int_{\epsilon_{0,min}}^{\epsilon_{0,KN}} \epsilon_0^{-\alpha_0} d\epsilon_0}{\int_{\epsilon_{0,min}}^{\epsilon_{0,max}} \epsilon_0^{-\alpha_0} d\epsilon_0} \simeq (\epsilon_{0,KN}/\epsilon_{0,max})^{-\alpha_0+1} = b^{\alpha_0-1}, \quad (5)$$

if rewrite the electron energy as  $b = 4\epsilon_{0,max}\gamma$  and have  $\epsilon_{0,min} \ll \epsilon_{0,max}$ . A useful approximation that interpolates to the Thomson limit for  $b \rightarrow 0$  and has good accuracy for  $0 < \alpha_0 < 1$  is then given by,

$$F_{KN} \simeq \frac{1}{(1+b)^{1-\alpha_0}}. \quad (6)$$

If we instead have  $\alpha_0 > 1$ , the Compton losses of the electrons are dominated by scatterings on the lowest energy photons available, at  $\sim \epsilon_{0,min}$ . We may then use the approximation,  $F_{KN} \simeq f_{KN}(\tilde{b} = 4\gamma\epsilon_{0,min})$ . If we further have  $4\gamma_{max}\epsilon_{0,min} < 1$ , then in fact all scatterings are effectively in the Thomson regime even if higher energy ambient photons are present and  $b_{max} > 1$ . To gauge the accuracy of approximations (3) and (6), we compare in Fig. 1 the approximate values of  $F_{KN}(b)$  to the exact ones for three different ambient photon spectra: mono-energetic, and power laws with  $\alpha_0 \equiv -d \ln u_{\epsilon_0} / d \ln \epsilon_0 = 0.0$  and  $0.5$ . From an analysis similar to that for the power law case, one can show that  $F_{KN}$  for a Planckian (thermal) distribution is well-approximated by treating the Planckian as a mono-energetic photon distribution with energy  $2.8kT$ .

## 2.2. Synchrotron energy losses vs. inverse-Compton energy losses

Noting that the rate of synchrotron losses in a tangled magnetic field of strength  $B$  is

$$|\dot{\gamma}|_{syn} = \frac{4c\sigma_T}{3m_e c^2} u_B \gamma^2 \quad (7)$$

where  $u_B = B^2/8\pi$  is the magnetic energy density, we have (see Eq.1)

$$\frac{\dot{\gamma}_{IC}}{\dot{\gamma}_{syn}} = q F_{KN} \quad (8)$$

where  $q \equiv u_0/u_B$ . Since  $F_{KN} < 1$  for any value of  $b$ , for  $q < 1$  the energy losses for all electrons are dominated by synchrotron radiation. For  $q > 1$ , the energy losses for electrons with  $\gamma < \gamma_s$  are dominated by inverse Compton scattering while losses for electrons with  $\gamma > \gamma_s$  are instead dominated by synchrotron radiation, where  $\gamma_s = b_s/4\epsilon_{0,max}$ , and  $b_s$  is the solution of the equation  $qF_{KN} = 1$ , plotted in Fig. 2. For a mono-energetic ambient photon spectrum (see Eq.3)

$$b_s \simeq q^{2/3} - 1, \quad (9)$$

while for a power-law spectrum with  $0 < \alpha_0 < 1$  (see Eq.6),

$$b_s \simeq q^{1/(1-\alpha_0)} - 1. \quad (10)$$

The relative role of the IC and synchrotron energy losses is illustrated in Fig. 3. We show there

$$\frac{\dot{\gamma}_{IC}}{\dot{\gamma}_{tot}} = \frac{qF_{KN}(b)}{1 + qF_{KN}(b)}, \quad (11)$$

and

$$\frac{\dot{\gamma}_{syn}}{\dot{\gamma}_{tot}} = \frac{1}{1 + qF_{KN}(b)}, \quad (12)$$

for three different spectra of the ambient radiation field, assuming that  $\dot{\gamma}_{tot} = \dot{\gamma}_{IC} + \dot{\gamma}_{syn}$ .

### 3. INVERSE-COMPTON EMISSIVITY

The inverse Compton emissivity for isotropically distributed electrons is

$$j_{\epsilon(IC)} = \int \frac{\partial P_{\epsilon(IC)}(\gamma)}{\partial \Omega} n_{\gamma} d\gamma, \quad (13)$$

where

$$\frac{\partial P_{\epsilon(IC)}(\gamma)}{\partial \Omega} = \frac{\partial \dot{N}_{sc}(\epsilon, \gamma)}{\partial \epsilon \partial \Omega} \epsilon m_e c^2, \quad (14)$$

is the IC-power per unit photon energy per solid angle per electron. For two particular cases, mono-directional beams of target photons and an isotropic radiation field, the respective scattering rates are given by Eqs. (A1) and (A4). Inserting them into Eq. (13) gives, for the beamed mono-energetic external radiation field,

$$\epsilon j_{\epsilon(IC)}(\theta) = \frac{3}{16\pi} c \sigma_T u_0 \left( \frac{\epsilon}{\epsilon_0} \right)^2 \int \frac{n_{\gamma}}{\gamma^2} f(\gamma, \epsilon, \epsilon_0, \theta) d\gamma, \quad (15)$$

and for the isotropic ambient radiation field,

$$\epsilon j_{\epsilon(IC)} = \frac{3}{16\pi} c \sigma_T u_0 \left( \frac{\epsilon}{\epsilon_0} \right)^2 \int \frac{n_{\gamma}}{\gamma^2} f_{iso}(\gamma, \epsilon, \epsilon_0) d\gamma, \quad (16)$$

where  $\theta$  is the scattering angle (the angle between the photon beam and the direction to the observer), the functions  $f(\gamma, \epsilon, \epsilon_0, \theta)$  and  $f_{iso}(\gamma, \epsilon, \epsilon_0)$  are given by Eqs. (A3) and (A7). These formulas can easily be generalized for any spectrum of external radiation field by replacing  $u_0$  by  $u_{\epsilon_0} d\epsilon_0$  and integrating them over  $\epsilon_0$ .

A useful first approximation for the IC spectrum (e.g., see Coppi & Blandford 1990) may be obtained by making the delta function approximation  $f(\epsilon, \gamma, \epsilon_0) \propto \delta[\epsilon - \bar{\epsilon}_{IC}(\gamma)]$ , where

$$\bar{\epsilon}_{IC}(\gamma, \theta) = \frac{\int \epsilon f(\gamma, \epsilon, \epsilon_0, \theta) d\epsilon}{\int f(\gamma, \epsilon, \epsilon_0, \theta) d\epsilon} \quad (17)$$

and

$$\bar{\epsilon}_{IC}(\gamma) = \frac{\int \epsilon f_{iso}(\gamma, \epsilon, \epsilon_0) d\epsilon}{\int f_{iso}(\gamma, \epsilon, \epsilon_0) d\epsilon} \quad (18)$$

are the average energies of photons produced by the scattering of photons of energy  $\epsilon_0$  by electrons with energy  $\gamma$ . A useful quantity to know when dealing with the KN regime is the electron's scattering inelasticity, i.e., the average fraction of the incident electron's energy that is transferred to the scattered photon:  $\mathcal{A} = \bar{\epsilon}_{IC}(\gamma)/\gamma$ . This is shown in Fig. 4 for the case of a mono-energetic ambient photon field.

Inserting the delta function approximation into Eqs. (15), and (16), we can rewrite the IC emissivities as

$$\epsilon j_{\epsilon(IC)}(\theta) \simeq \frac{n_\gamma \gamma}{4\pi} |\dot{\gamma}|_{IC} m_e c^2 \chi(\gamma, \theta) \frac{d \ln \gamma}{d \ln \bar{\epsilon}_{IC}(\theta)}, \quad (19)$$

and

$$\epsilon j_{\epsilon(IC)} \simeq \frac{n_\gamma \gamma}{4\pi} |\dot{\gamma}|_{IC} m_e c^2 \frac{d \ln \gamma}{d \ln \bar{\epsilon}_{IC}}, \quad (20)$$

respectively, where

$$\chi(\gamma, \theta) = \frac{\int f(\epsilon, \epsilon_0, \gamma, \theta) \epsilon d\epsilon}{\int f_{iso}(\epsilon, \epsilon_0, \gamma) \epsilon d\epsilon} \equiv \frac{\bar{\epsilon}_{IC}(\gamma, \theta)}{\bar{\epsilon}_{IC}(\gamma)}. \quad (21)$$

Note that in the Thomson limit,  $\bar{\epsilon}_{IC} \propto \gamma^2$ , so that  $d \ln \gamma / d \ln \bar{\epsilon}_{IC} = 1/2$ , while in the KN limit,  $\bar{\epsilon}_{IC} \sim \gamma$  so that  $d \ln \gamma / d \ln \bar{\epsilon}_{IC} = 1$ .

We can make an analogous approximation for the synchrotron emissivity, provided that the magnetic fields are isotropic and  $\gamma_{max} < B_{cr}/(4B)$ . We have then,

$$\epsilon j_{\epsilon(syn)} \simeq \frac{n_\gamma \gamma}{4\pi} |\dot{\gamma}|_{syn} m_e c^2 \frac{d \ln \gamma}{d \ln \bar{\epsilon}_{(syn)}} = \frac{1}{2} \frac{n_\gamma \gamma}{4\pi} |\dot{\gamma}|_{syn} m_e c^2 \quad (22)$$

where  $\bar{\epsilon}_{syn} = (4/3)\gamma^2(B/B_{cr})$  and  $B_{cr} \equiv 2\pi m_e^2 c^3 / (he) \simeq 4.4 \times 10^{13}$  Gauss.

#### 4. STEADY-STATE ELECTRON ENERGY DISTRIBUTION

Under the assumptions that the time scales for the acceleration of individual electrons are much shorter than time scales of their energy losses, that electrons do not escape from the cooling region, and that they also do not suffer adiabatic losses, the evolution of the electron energy distribution,  $n_\gamma$ , can be described by the integro-differential equation (Blumenthal & Gould 1970)

$$\frac{\partial n_\gamma}{\partial t} = -\frac{\partial}{\partial \gamma} (n_\gamma |\dot{\gamma}|) - n_\gamma \int_1^\gamma C(\gamma, \gamma') d\gamma' + \int_\gamma^{\gamma_{max}} n_\gamma C(\gamma', \gamma) d\gamma' + Q, \quad (23)$$



where  $|\dot{\gamma}|$  is the energy loss rate due to loss processes that may be approximated as being continuous, e.g., synchrotron radiation,  $C(\gamma, \gamma')$  is the probability per unit time for Compton scattering of an electron with energy  $\gamma$  to energy  $\gamma'$ , and  $Q$  is the electron injection function, i.e. the electron production rate per unit time, per energy and per volume. The transition rates  $C(\gamma, \gamma')$  have been derived by Jones (1968) for a mono-energetic ambient radiation field, and by Zdziarski (1988) for power-law ambient radiation fields.

To illustrate in a simple way the effects of KN corrections, we will use a continuity version of the kinetic equation

$$\frac{\partial n_\gamma}{\partial t} = -\frac{\partial}{\partial \gamma} (n_\gamma |\dot{\gamma}|_{tot}) + Q, \quad (24)$$

despite the fact that in the KN regime the fractional electron energy losses per scattering are *not* negligible (see Fig. 4). Such a simplification can be justified by noting that the results obtained by Zdziarski (1989) show that the electron distributions obtained by using the exact integro-differential equation versus the continuity equation are qualitatively very similar and that significant differences (up to a factor few) occur only if both the electron injection function and the ambient radiation field are mono-energetic. In the cases studied here, the differences are further reduced by the increasingly important role of the (continuous) synchrotron energy losses at the highest energies, particularly if  $b_{max} > b_s$ . We demonstrate this explicitly in Fig. 5-7 where we compare the results of exact calculations made using the code of Coppi (1992) with the approximate results obtained by treating Compton losses continuously in that code. For many applications that do not involve fitting data and thus do not require very high accuracy, the continuous energy loss approximation should suffice.

A steady-state solution of the continuity equation,  $\partial n_\gamma / \partial t = 0$ , is

$$n_\gamma = \frac{1}{|\dot{\gamma}_{tot}|} \int_\gamma Q d\gamma = \frac{3m_e c}{4\sigma_T u_B} \frac{\int_\gamma Q d\gamma}{\gamma^2 (1 + qF_{KN})}. \quad (25)$$

where we assume that electron energy losses are dominated by inverse Compton process and by synchrotron radiation, i.e. that

$$|\dot{\gamma}_{tot}| = |\dot{\gamma}_{syn}| + |\dot{\gamma}_{IC}| = \frac{4c\sigma_T u_B}{3m_e c^2} \gamma^2 (1 + qF_{KN}). \quad (26)$$

For  $b_{max} \gg b_s$  and  $q \gg 1$ , the steady-state then distribution has two asymptotes: one for  $b \ll 1$ , where electron energy losses are dominated by Thomson scatterings, i.e.  $F_{KN} = 1$ ; and one for  $b_s \ll b \ll b_{max}$ , where electron energy losses are dominated by synchrotron radiation, i.e.  $qF_{KN} \ll 1$ . The respective equilibrium electron distributions are:  $\gamma^2 n_\gamma \propto \int_\gamma Q d\gamma / (1 + q)$  and  $\gamma^2 n_\gamma \propto \int_\gamma Q d\gamma$ . For  $1 < b < b_s$ , despite the decrease of the KN

cross section, electron energy losses are still dominated by the IC process and the electron distribution is  $\gamma^2 n_\gamma \propto \int_\gamma Q d\gamma / (q F_{KN})$ .

For a rapid acceleration mechanism that produces a power law electron injection spectrum,  $Q \propto \gamma^{-p}$ , with  $p > 1$ , the two asymptotes of the steady state distribution (for  $b \ll 1$ , and  $b \gg b_s$ ) are power laws with the same spectral index,  $s = p + 1$ , where  $s \equiv -d \ln n_\gamma / d \ln \gamma$ . For  $1 \ll b \ll b_s$ , i.e., for  $\gamma_{KN} < \gamma < \gamma_s$ , the electron distribution is *harder* than in the asymptotic regions, with a spectral index reaching  $s = p + 1 + \Delta s$ , where  $\Delta s \simeq d \ln F_{KN} / d \ln \gamma < 0$ . Using the analytical approximations for  $F_{KN}$  given in §2 and going to the limit  $q \gg 1$ , one finds that for ambient radiation fields with mono-energetic or very sharply peaked photon energy distributions,  $\Delta s \simeq -1.5$ , while for softer external fields, with  $\alpha_0 > 0.0$ ,  $\Delta s \simeq \alpha_0 - 1$ . When  $q \lesssim 10^3$ , the maximum hardening,  $\Delta s$ , of the electron distribution is a function of  $q$  and decreases with decreasing  $q$ . (See Fig. 8 for an example of how the corresponding hardening of the electron synchrotron depends on  $q$ .) Note that to the extent the continuous Compton cooling approximation is a good one, this result is independent of the injection index  $p$ . Of course, for  $b_{max} < b_s$  the electron energy distribution will not have the maximum deviation possible from the Thomson-limit ( $b \ll 1$ ) asymptote and  $\Delta s$  may not reach its maximum value. In this case, the KN induced bump or “excess” at the high energy end of the electron distribution is correspondingly less prominent. This is demonstrated in Fig. 5, where the electron distribution is computed for four different values of  $b_{max}$ .

## 5. SPECTRA

### 5.1. Klein-Nishina effects

Examples of the steady-state electromagnetic spectra produced for the case of power-law electron injection function are shown in Figs. 6 and 7. The IC spectra are computed assuming an isotropic ambient radiation field. The characteristic photon energies marked on the figures have the following definitions (see Eq. 18):  $\epsilon_{IC,KN} \equiv \bar{\epsilon}_{IC}(\gamma_{KN})$ ;  $\epsilon_{IC,s} \equiv \bar{\epsilon}_{IC}(\gamma_s)$ ;  $\epsilon_{syn,KN} \equiv \bar{\epsilon}_{syn}(\gamma_{KN})$ ;  $\epsilon_{syn,s} \equiv \bar{\epsilon}_{syn}(\gamma_s)$ ; and  $\epsilon_+ \equiv 2/\epsilon_{0,max}$ , which is the approximate threshold energy for photon-photon pair production on the ambient photon distribution.

As one can see, the high energy portions of the inverse-Compton (IC) and synchrotron spectra behave very differently. The IC spectra do not change very much after crossing  $\epsilon_{IC,KN}$ . This is because for  $q \gg 1$ , Compton scattering is still dominating the cooling of the electrons responsible for IC photons at  $\epsilon \gtrsim \epsilon_{IC,KN}$ . Even though those electrons scatter in the KN regime, the decreased efficiency of Compton scattering is compensated by the corresponding increase in their equilibrium density, as discussed in Zdziarski & Krolik (1993).

As one moves to higher photon energies, however, synchrotron cooling becomes relatively more important for the electrons responsible these IC photons. Eventually, when the energy of the relevant electrons exceeds  $\gamma_s$ , synchrotron cooling rapidly dominates and the fraction of the electron’s energy going into the Compton component plummets. The result is a sharp steepening or break of the IC spectrum at energy  $\epsilon_{IC,s}$ , which is *independent* of the maximum electron energy  $\gamma_{max} > \gamma_s$ .

When one instead considers synchrotron emission, the hardening of the electron distribution at  $\gamma > \gamma_{KN}$  is directly reflected in the synchrotron spectrum. The result is a synchrotron spectrum that can harden dramatically at  $\epsilon > \epsilon_{syn,KN}$ , forming a synchrotron “bump” if  $b_{max} < b_s$ . (Note that if  $q \gg 1$ , the hardening of the synchrotron component can already be noticeable at even lower energies,  $\sim \bar{\epsilon}_{syn}(0.1\gamma_{KN})$ .) For  $b_{max} \gg b_s$ , the synchrotron spectrum at  $\epsilon > \epsilon_{syn,s}$  asymptotes to a spectrum with the same slope as the low energy (Thomson regime) asymptote but with a normalization that is a factor  $q$  higher.

An interesting consequence of the very different behaviors of the high energy portions of IC and synchrotron spectra is that for the case of a flat electron injection spectrum ( $p < 2$ ) with  $b_{max} > b_s$ , the luminosity of the synchrotron peak – located around  $\epsilon_{syn,max} \equiv \bar{\epsilon}_{syn}(\gamma_{max})$  – will exceed the luminosity of the IC peak – located around  $\epsilon_{IC,s}$ , no matter how large we make  $q$ . This dominance of the synchrotron component, even though  $q = 30 \gg 1$ , is demonstrated in Fig. 7.

All the spectral features just described can be reproduced analytically, by using the equations

$$\epsilon j_{\epsilon(IC)} \simeq \frac{m_e c^2}{4\pi} \frac{q F_{KN}}{1 + q F_{KN}} \gamma \int_{\gamma} Q d\gamma \frac{d \ln \gamma}{d \ln \bar{\epsilon}_{IC}}, \quad (27)$$

and

$$\epsilon j_{\epsilon(syn)} \simeq \frac{1}{2} \frac{m_e c^2}{4\pi} \frac{1}{1 + q F_{KN}} \gamma \int_{\gamma} Q d\gamma, \quad (28)$$

which are obtained after insertion of Eq. (25) into Eqs. (20) and (22), respectively. For  $\gamma_{max} \gg \gamma_s$  and  $q \gg 1$ , the latter implying  $b_s \gg 1$  i.e.  $\gamma_s \gg \gamma_{KN}$ , the IC and synchrotron spectra can be characterized as the superposition of three components produced by electrons with:  $\gamma \ll \gamma_{KN}$ ;  $\gamma_{KN} \ll \gamma \ll \gamma_s$ ; and  $\gamma_s \ll \gamma \ll \gamma_{max}$ . These components are:

$$\frac{4\pi \epsilon j_{\epsilon(IC)}}{m_e c^2} \sim \gamma \int_{\gamma} Q d\gamma \times \begin{cases} 1/2 & \text{if } \epsilon \ll \epsilon_{IC,KN} \\ 1 & \text{if } \epsilon_{IC,KN} \ll \epsilon \ll \epsilon_{IC,s} \\ q F_{KN} & \text{if } \epsilon_{IC,s} \ll \epsilon \ll \epsilon_{IC,max} \end{cases}, \quad (29)$$

where  $\gamma \simeq \sqrt{(3/4)(\epsilon/\epsilon_{0,max})}$  if  $\epsilon \ll \epsilon_{IC,KN}$ , and  $\epsilon \simeq \gamma$  if  $\epsilon \gg \epsilon_{IC,KN}$ ; and

$$\frac{4\pi\epsilon j_{\epsilon(syn)}}{m_e c^2} \sim \gamma \int_{\gamma} Q d\gamma \times \begin{cases} 1/(2q) & \text{if } \epsilon \ll \epsilon_{syn,KN} \\ 1/(2qF_{KN}) & \text{if } \epsilon_{syn,KN} \ll \epsilon \ll \epsilon_{syn,s} \\ 1/2 & \text{if } \epsilon_{syn,s} \ll \epsilon \ll \epsilon_{syn,max} \end{cases}, \quad (30)$$

where  $\gamma = \sqrt{3\epsilon B_{cr}/(4B)}$ .

For electron injection  $Q \propto \gamma^{-p}$  and  $p > 1$ , the various components are power laws, i.e., we have:

$$\frac{4\pi\epsilon j_{\epsilon(IC)}}{m_e c^2} \propto \begin{cases} \epsilon^{-p/2} & \text{if } \epsilon \ll \epsilon_{IC,KN} \\ \epsilon^{-(p-1)} & \text{if } \epsilon_{IC,KN} \ll \epsilon \ll \epsilon_{IC,s} \\ \epsilon^{-(p-1+\delta\alpha)} & \text{if } \epsilon_{IC,s} \ll \epsilon \ll \epsilon_{IC,max} \end{cases}, \quad (31)$$

where  $\delta\alpha \sim 1.5$  for  $\alpha_0 < -1$ , and  $\delta\alpha \sim 1 - \alpha_0$  for  $0 < \alpha_0 < 1$ , while

$$\frac{4\pi\epsilon j_{\epsilon(syn)}}{m_e c^2} \propto \begin{cases} \epsilon^{-p/2} & \text{if } \epsilon \ll \epsilon_{syn,KN} \\ \epsilon^{-(p/2+\Delta\alpha)} & \text{if } \epsilon_{syn,KN} \ll \epsilon \ll \epsilon_{syn,s} \\ \epsilon^{-p/2} & \text{if } \epsilon_{syn,s} \ll \epsilon \ll \epsilon_{syn,max} \end{cases}, \quad (32)$$

where  $\Delta\alpha = -(d \ln(1/F_{KN})/d \ln \epsilon)|_{b\alpha\epsilon^{1/2}}$ . For  $\alpha_0 < -1$ ,  $\Delta\alpha \sim -0.75$ , while for  $0 < \alpha_0 < 1$ ,  $\Delta\alpha \sim -(1 - \alpha_0)/2$ . We should emphasize here, that estimation of the hardening of synchrotron spectrum slope in the band  $[\epsilon_{syn,KN}; \epsilon_{syn,s}]$  is very crude and corresponds to its maximum value, which as noted previously, can be reached only for  $q \gtrsim 10^3$ . As shown in Fig. 8, the synchrotron spectral hardening will be weaker for lower values of  $q$ .

Although we have only presented and discussed emission spectra computed for an isotropic ambient radiation field, we would like to emphasize, that with our generic assumption of isotropic distribution of electrons, the electron energy losses, as well, as the distribution of electrons (Eq. 25) and their synchrotron emissivity (Eq. 22), do not depend on angular distribution of ambient radiation field. Hence, in the case of a beamed ambient radiation field the IC spectrum can be simply computed from Eq. (15) or (19) by using there the electron distribution given by Eq. (25). In Fig. 10 we show such spectra for three different scattering angles and compare them with the one computed for the isotropic ambient radiation field. One can see that the deeper one is in the KN regime, the weaker is anisotropy of the scattered radiation. Suppression of the anisotropy is caused by the recoil effect.

## 5.2. Further effects that may modify the observed spectrum

To highlight the spectral effects caused by the modification of the electron energy distribution due to Compton scatterings in the KN regime, we have considered only spectra

produced in the fast electron cooling regime, and we have ignored possibly important processes such as photon-photon pair production and synchrotron self-Compton radiation. We also did not consider effects due to the relativistic propagation of the source, which is important in objects like blazars. We discuss below how our results can be affected by the inclusion of some of these complications.

*The fast vs. slow cooling regime*

Assuming that electron energy losses are dominated by radiative processes, the cooling time scale for an electron of energy  $\gamma$  is (see Eq. 26)

$$t_c \equiv \frac{\gamma}{|\dot{\gamma}|} = \frac{3m_e c}{4\sigma_T u_B \gamma (1 + qF_{KN})}. \quad (33)$$

For sources with a finite (comoving frame) lifetime  $t_Q$ , the only electrons that have time to cool significantly are those with  $t_c < t_Q$ . Looking first at the Thomson limit ( $\gamma \lesssim \gamma_{KN}$ ) of this expression, one finds the usual result that only electrons with  $\gamma > \gamma_c$  have time to cool, where

$$\gamma_c = \frac{3m_e c}{4\sigma_T u_0 t_Q} \quad (34)$$

for  $q \gg 1$ . The number density of electrons at a given energy that can accumulate in the source is roughly  $Q(\gamma) \times \min[t_c(\gamma), t_Q]$ . For power law electron injection, the electron energy distribution of electrons therefore hardens by  $\Delta s = 1$  for  $\gamma < \gamma_c$ , leading to a hardening of the synchrotron or Compton spectrum by  $\Delta\alpha = 0.5$ .

For  $\gamma > \gamma_{KN}$ ,  $q \gg 1$ , and a mono-energetic ambient photon distribution, the the cooling time increases for  $\gamma > \gamma_{KN}$ , reaching a local maximum at  $\gamma \approx \gamma_s$ , when synchrotron cooling begins to dominate. Efficient KN cooling therefore requires  $t_c(\gamma_s) < t_Q$ . From Eq. (33), we have

$$t_c(\gamma_s) = \frac{3m_e c}{8\sigma_T u_B \gamma_s} = \frac{3m_e c \epsilon_0 q}{2\sigma_T u_0 b_s}. \quad (35)$$

Hence, fast cooling in the KN regime requires

$$\frac{q}{b_s} < \frac{2\sigma_T u_0 t_Q}{3\epsilon_0 m_e c} \quad (36)$$

or, equivalently using  $b_s \sim q^{2/3}$  for  $1 \ll q \lesssim 10^3$ ,

$$q < \left( \frac{2\sigma_T u_0 t_Q}{3\epsilon_0 m_e c} \right)^3. \quad (37)$$

Of course, if we have  $b_{max} < b_s$ , the upper limit on  $q$  is correspondingly weaker.

For a power law photon distribution with  $0 \lesssim \alpha_0 \lesssim 1$ , we may use Eq. (33) and approximation (6) to show that  $t_c \sim \gamma^{-\alpha_0}$ . For  $\alpha_0 > 0$ , this is a monotonically decreasing function of  $\gamma$ , so fast cooling throughout the KN regime is simply guaranteed by the condition  $t_c(\gamma_{KN}) \leq t_Q$ , or equivalently  $\gamma_{KN} > \gamma_c$ . This can be translated into the following requirement on the energy density of the external radiation field,

$$u_0 > \frac{3m_e c}{4\gamma_{KN}\sigma_T t_Q} = \frac{3m_e c \epsilon_0}{\sigma_T t_Q}. \quad (38)$$

For a photon distribution that is harder than  $\alpha_0 = 0$  or softer than  $\alpha_0 = 1$ , the condition for a mono-energetic radiation field, i.e., we require  $t_c(\gamma_s) \leq t_Q$ .

### *Photon-photon pair production*

Because (a) the cross-section for photon-photon pair production is similar in magnitude to that for Compton scattering, and (b) the photon threshold energy for pair production,  $\epsilon_+ \sim 1/\epsilon_{0,max}$ , is almost the same as the electron energy  $\gamma_{KN} \sim 1/\epsilon_{0,max}$ , it is often stated that strong pair production is unavoidable in sources where KN effects are important. This is not always true, however.

First, in many applications a better estimate for the threshold energy is in fact  $\epsilon_+ = 2/\epsilon_{0,max}$ . Moreover, KN effects are actually important at energies well below  $1/\epsilon_{0,max}$ , i.e., at  $\gamma < \gamma_{KN} = 1/4\epsilon_{0,max}$ . Furthermore, from Fig. 4.,  $\mathcal{A}(\gamma_{KN}) \sim 0.1 - 0.3$ , so that an electron of energy  $\gamma_{KN}$  Compton actually upscatters photons to typical energies  $\epsilon_{IC,KN} = \mathcal{A}_{KN}\gamma_{KN} \ll \epsilon_+$ . Taking  $\mathcal{A}$  at larger energies to be  $\sim 0.5$ , we see that we in fact need a source with  $b_{max} > b_+ = \gamma_+/\gamma_{KN} \simeq 16$ . Since KN distortions of the electron spectrum already produce visible distortions in the synchrotron spectrum for electron energies  $b \sim 0.1$ , this means there is a factor  $\sim 100$  in electron energy for which KN corrections are important but pair production is not possible. Since  $\bar{\epsilon}_{syn} \propto b^2$ , this corresponds to a factor  $10^4(!)$  in synchrotron frequency.

Second, even if we have  $b_{max} \gtrsim b_+$ , pair production may still not be important. When one includes the effects of synchrotron cooling, left out of KN pair production studies such as Zdziarski (1988), we have seen that one obtains a strong break at  $\epsilon_{IC,s}$  corresponding to the electron energy  $b_s$  where synchrotron cooling starts to dominate. Thus, if  $b_+ < b_{max}$  but  $b_+ > b_s$ , pair production occurs but the luminosity of the pairs that are produced (and the spectral distortions they induce) will not be bolometrically important. For a mono-energetic photon distribution,  $b_s \simeq q^{2/3}$ , and one thus has  $b_s < b_+$  for any  $q \lesssim 60$ , *independent* of the actual value of the maximum electron energy,  $b_{max}$ , e.g., see Fig. 6a and Fig. 7. Note, though, that for an ambient photon distribution that is not mono-energetic, e.g., a power law with  $\alpha_0 \gtrsim -0.5$ , KN effects are not as strong as for the mono-energetic case because lower energy photons that scatter in the Thomson regime are available. The spectral break

due to  $\epsilon_{IC,s}$  therefore occurs at higher energy and pair production can be important for much lower  $q$ , e.g., see Fig. 6b.

Even if pair production is energetically possible, the preceding discussion says nothing about whether the optical depth to pair production  $\tau_{\gamma\gamma}$  actually exceeds unity, and it ignores the effects of photon anisotropy (which raise the pair production threshold). In a realistic source, the extent and geometry of the external radiation field must be taken into as well as its absolute intensity. In galactic pulsar wind applications, for example, the ambient radiation field due to the companion star is often highly anisotropic in the source region of interest. In the most general case,  $\tau_{\gamma\gamma}$  must be treated as a free parameter. In particular, if the source region has an effectively infinite lifetime and is not expanding, which would induce adiabatic losses, we are essentially free to choose as low an external field energy density as we like without violating the fast KN cooling constraints discussed above. (If we choose too low an external energy density, of course, higher order like bremsstrahlung start to be important.) If the source is not static, though, there are interesting limits we can place on  $\tau_{\gamma\gamma}$  if we demand efficient KN cooling. For example, consider a source of size  $R$  with a characteristic lifetime or expansion timescale  $\sim R/c$ . For simplicity, assume also that the radiation field is mono-energetic. Then, taking  $\tau_{\gamma\gamma} \simeq 0.2n_0\sigma_T R$  where  $n_0 = u_0/\epsilon_0$  and using the fast-cooling condition of eqn. (35), we have

$$\tau_{\gamma\gamma} \gtrsim \frac{3}{10}q^{1/3}. \quad (39)$$

This implies, for example, that we can be in the fast KN regime and still have  $\tau_{\gamma\gamma} < 1$  for  $q \lesssim 37$ .

### *Synchrotron-Self Compton (SSC) Effects*

In addition to the external ambient photons, synchrotron photons from the cooling electrons will always be present in the source. The synchrotron photons spectrum is typically broad and extends to low energies, i.e., it is not well-approximated by a mono-energetic photon distribution. The SSC spectrum produced by synchrotron photon upscattering can thus be quite different in shape from the spectrum produced by the upscattering of external photons, in particular it may extend to higher energies. This may be important in certain applications. For a very weak external radiation field or a very compact source, the Compton losses due the synchrotron photons may in fact dominate over the losses due to the external field, leading to significant changes in the equilibrium electron distribution and thus the emergent spectrum. These will be explored further in a subsequent paper. The analysis is more complicated than in the present case because the target radiation field and the electron distribution must be determined simultaneously and self-consistently. (As we have seen, many quantities depend sensitively on the details of the low-energy photon spectrum.)

Nonetheless, the main effects described here still occur, e.g., the synchrotron spectrum is harder than expected from a Thomson-limit analysis and for sufficiently high electron injection energies, there will be an energy  $\gamma_s$  above which synchrotron losses dominate, leading to a corresponding break in the Compton spectrum.

*Relativistic source propagation effects*

If a source is moving with relativistic speed (bulk Lorentz factor  $\Gamma \gg 1$ ), and the external radiation field in such a frame is isotropic, and with an energy density  $u_0$  peaked at photon energies  $\sim \epsilon_0$ , then in the source rest frame, the energy density of the external radiation is  $\Gamma^2$  times larger and the energies of seed photons are  $\Gamma$  times higher. Then the rest frame quantities relevant to our discussion of KN effects are  $b = 4\Gamma\gamma\epsilon_0$ , and, in particular,  $\gamma_{KN} \simeq 1/(4\Gamma\gamma\epsilon_0)$ , and  $q \simeq \Gamma^2 u_0/u_B$ . Since for  $\Gamma \gg 1$  the head-on approximation applies, the IC Compton emissivity can be computed using Eq.(15) with

$$\cos \theta = -\cos \psi'_{obs} = -\frac{\cos \psi_{obs} - \beta}{1 - \beta \cos \psi_{obs}}, \quad (40)$$

where  $\psi'_{obs}$  is the angle between the jet axis and the direction to the observer in the co-moving frame while  $\psi_{obs}$  is the same angle but as measured in the lab frame. The observed source flux is then

$$\epsilon_{obs} F_{\epsilon_{obs}} = \frac{\mathcal{D}^4 \int \epsilon j_{\epsilon}(\theta) dV}{d_L^2} \quad (41)$$

where  $\epsilon_{obs} = \epsilon \mathcal{D}/(1+z)$ ,  $\mathcal{D} = 1/[\Gamma(1 - \beta \cos \psi_{obs})]$  is the Doppler factor,  $d_L$  is the distance (luminosity distance for cosmological objects),  $z$  is the redshift, and  $V$  is the volume of the source as measured in its rest frame. The lifetime of the source measured in the lab frame is  $\Gamma t_Q$ .

## 6. APPLICATIONS

### 6.1. Blazars

The clearest and probably most numerous examples of high- $q$  (radiation dominated) non-thermal sources are the powerful blazars where we think we are seeing emission from a relativistic jet oriented towards us. In many of these objects, the bolometric luminosity is strongly dominated by  $\gamma$ -rays (von Montigny et al. 1995; Mukherjee et al. 1997). A day-week variability time scales suggest that these sources are located at (sub-)parsec distances from the center. There, the external radiation field, as viewed in the jet co-moving frame, is dominated by the powerful Broad Emission Line (BEL) region radiation. For



$u_0 \simeq L_{BEL}/(4\pi r_{BEL}^2 c)$  and  $u_B \simeq L_B/(\pi(r\theta_j)^2 c\Gamma^2)$ ,

$$q(r \sim r_{BEL}) \simeq \frac{\Gamma^2 u_0}{u_B} \simeq 25 \frac{L_{BEL,45}(\Gamma/10)^2(\Gamma\theta_j)^2}{4L_{B,45}}, \quad (42)$$

where  $L_B$  is the magnetic energy flux carried by the jet and  $\theta_j = R/r$  is the half-opening angle of a jet.

Let us determine now the values of  $\gamma_{KN}$  and  $\gamma_s$  and of the corresponding IC and synchrotron photon energies for such an external radiation field, assuming that  $q \gg 1$  and  $\gamma_{max} > \gamma_s$ . Noting that the energies of broad emission lines peak around  $\sim 10\text{eV}$  ( $\epsilon_0 \approx 2 \times 10^{-5}$ ) and that they are seen in the jet co-moving frame as boosted by a factor  $\sim \Gamma$ , i.e.  $b = 4\epsilon_0\Gamma$ , we have

$$\gamma_{KN} = \frac{1}{4\epsilon_0\Gamma} \sim 10^3(\Gamma/10)^{-1} \quad (43)$$

and

$$\gamma_s = b_s\gamma_{KN} \sim 10^4(q/30)^{2/3}(\Gamma/10)^{-1} \quad (44)$$

These electrons Comptonize external photons up to average energies

$$\epsilon_{IC,KN}^{obs} \simeq \mathcal{A}_{KN}\gamma_{KN}\mathcal{D} \sim 2 \times 10^3(\mathcal{A}_{KN}/0.14)(\mathcal{D}/\Gamma) (\sim 1\text{GeV} \dots), \quad (45)$$

and

$$\epsilon_{IC,s}^{obs} \simeq \mathcal{A}_s\gamma_s\mathcal{D} \simeq 6 \times 10^4(\mathcal{A}_s/0.5)(q/30)^{2/3}(\mathcal{D}/\Gamma) (\sim 30\text{GeV} \dots), \quad (46)$$

and produce synchrotron photons with average energies

$$\epsilon_{syn,KN}^{obs} = \frac{4}{3}\gamma_{KN}^2 \frac{B}{B_{cr}}\mathcal{D} \sim 2 \times 10^{-7} \frac{L_{B,45}^{1/2}(\mathcal{D}/\Gamma)}{R_{BEL,18}(\Gamma/10)} (\sim 3 \times 10^{13}\text{Hz} \dots), \quad (47)$$

$$\epsilon_{syn,s}^{obs} = b_s^2 \epsilon_{syn,KN}^{obs} \simeq q^{4/3} \epsilon_{syn,KN}^{obs} \sim 2 \times 10^{-5} (q/30)^{4/3} \frac{L_{B,45}^{1/2}(\mathcal{D}/\Gamma)}{R_{BEL,18}(\Gamma/10)} (\sim 3 \times 10^{15}\text{Hz} \dots). \quad (48)$$

Hence, sources with  $q \gg 1$ ,  $1 < b_{max} < b_s$  and power-law electron injection should produce synchrotron ‘‘bumps’’ peaking in the IR-UV spectral band, with the closer a given  $b_{max}$  is to  $b_s$ , the more prominent the bump. As discussed, the presence of ‘‘excess’’ synchrotron emission (the bump) in this case is simply due to KN effects and should not be interpreted as indicating the presence of a new electron acceleration component or a hardening of the low energy injection spectrum.

We have just estimated the electron injection parameters that would put a luminous blazar into the KN regime studied here. Are there any blazars that actually populate this

region of parameter space? Since for even the brightest blazars, EGRET could not detect gamma-rays much beyond 1 GeV, the extension of the electron energy distribution into KN regime cannot be established using EGRET data. However, quite significant constraints on the high energy tails of the electron energy distribution are provided by observations of their synchrotron spectra. In the study of Padovani et al. 2003, about half of the objects in their sample of powerful blazar objects have synchrotron spectra peaking at  $\nu > 3 \times 10^{13}$  Hz, which implies  $b > 1$ . In most cases the spectra steepen in the UV band, indicating an injection function with a cutoff or break at  $b \sim$  a few, i.e., KN effects may be moderately important. There are few of these blazars, though, that have a synchrotron peak clearly located in the UV to soft X-ray band and may have  $b_{max} \gg 1$ . For these objects, assuming the external BEL radiation field is dominant with the characteristics described above, we then predict a high energy spectral break of the IC component at  $\epsilon_{IC,s} \sim 30$  GeV, independent of the observed synchrotron cutoff energy (i.e.,  $b_{max}$ ) provided that it is sufficiently large. If the electron injection spectrum for these objects is not unusually soft, i.e., we have  $p \lesssim 3$ , then as shown in Fig. 6-8, for example, a significant fraction of their bolometric luminosity actually emerges in the synchrotron component. In particular, their IC luminosity should be comparable to their synchrotron luminosity, i.e., they would *not* be gamma-ray loud objects (with  $L_{IC}/L_{syn} \gg 1$ ).

It would be very convenient if powerful blazars had gamma-ray spectra extending to TeV energies, e.g., they would provide very bright sources that could be used to constrain the intensity of the extragalactic background light via the absorption of their gamma-rays (Coppi & Aharonian 1999). Unfortunately, for the BEL parameters we have used, this is impossible unless  $q$  is extremely (and implausibly) large. One caveat to this conclusion is that we have not included SSC effects in our estimates, and because the synchrotron emission is much broader in energy than the BEL one,  $\gamma_s$  and  $\epsilon_{IC,s}$  could move to higher values. Note, though, that  $\epsilon_+$ , the energy above which pair production on the BEL becomes possible, is only  $\simeq 50$  GeV. Strong Compton TeV emission therefore seems unlikely unless it occurs far from the BEL and the typical ambient photon energy is in the near-infrared range.

## 6.2. Micro-blazars?

Only two or three EGRET sources have been identified with micro-quasars (Paredes et al. 2000; Massi et al. 2004; Combi et al. 2004). The fact that these objects are High Mass X-Ray Binary (HMXB) systems containing massive and very luminous companion stars strongly suggests a Compton origin for their  $\gamma$ -rays. As in blazars, the EGRET observations unfortunately do not provide constraints on  $\gamma_{max}$  for these objects. Furthermore, because these sources are relatively weak and completely dominated in the optical/UV band

by radiation from the companion stars, their synchrotron component cannot be identified. However, GRS 1915+105 proves that XRB have the ability to produce much more powerful and relativistic jets (Fender & Belloni 2004) than in the sources just mentioned. If such a powerful jet were to occur in an HMXB and it pointed toward us, we would see a *micro-blazar*, with relativistically boosted non-thermal radiation dominating over all spectral bands (Georganopoulos, Aharonian, & Kirk 2002). Since the spectra of HMXB companion stars peak at  $\sim 10$  eV, the same value for the BEL in quasars, the values of  $\gamma_{KN}$  and  $\gamma_s$ , and of  $\epsilon_{IC,KN}$  and  $\epsilon_{IC,s}$  are of the same order as for blazars and, therefore, like blazars, they are expected to be GeV emitters and not strong TeV emitters. Due to the much stronger magnetic fields in micro-quasar jets, the synchrotron spectral bumps, produced if  $b_{max} \gg 1$ , are predicted to peak in the UV/soft X-ray band. Hence, if some of the ULX (Ultra-Luminous X-ray) sources are in fact micro-blazars pointed at us, they should be strong  $\gamma$ -ray emitters (Georganopoulos *et al.* 2002).

However, we must remember, that very large  $q$  is available only on size scales comparable to those of the binary system. For electron acceleration occurring well down the jet, outside the binary system, the companion star radiation chases the relativistically moving emission region from behind and its energy density is thus Doppler deboosted when viewed in the jet frame. (The energy density of the companion star radiation field will be further reduced by the usual factor,  $\propto 1/r^2$  where  $r$  is the distance from the binary, but this effect can be canceled out by the fact that the magnetic field energy in a conically expanding jet also drops as  $1/r^2$ .) Closer in to the central object, jets typically have much stronger magnetic fields and, therefore, synchrotron radiation will dominate electron energy losses, even in the Thomson regime. In this case the IC spectrum is expected to break at  $\epsilon_{IC,KN}$ , i.e.,  $\sim 1$  GeV. This would be the case if, as in blazars, the jet energy is dissipated at  $10^{3-4}(r/r_g)$  where  $r_g$  is the gravitational radius of the compact object, i.e., on scales  $10^3$  times smaller than the typical size of an XRB system.

It should be noted that because the radiation field of the companion star is not symmetric about the jet axis, detailed computations of the non-thermal spectra from XRB require the integration of emissivities given by Eq. (15) over the energy distribution of the external radiation field, taking into account that in the source comoving frame, the radiation is boosted by a Doppler factor that depends on the direction of the incoming photons (Khangulian & Aharonian 2005). In other words, the exact geometry of the system is important.

### 6.3. Pulsars in HMXB

PSR B1259-63 and PSR J0045-73 provide examples of non-accreting binary pulsars with massive companions (Johnston et al. 1992; Kaspi et al. 1994); and PSR B1259-63 was recently identified as a TeV source (Aharonian et al. 2005). Ball and Kirk (2000) envisaged two scenarios for production of high energy radiation in such systems, Comptonization of the radiation field of the companion luminous star directly by the pulsar ultra-relativistic wind (i.e., a bulk-Compton scenario) or by particles accelerated in the terminal wind shock formed due to the confinement of the pulsar wind by the wind from the companion star. Since for finite values of  $q \gg 1$ , the IC spectrum has a high energy break at  $\epsilon_{IC,br} = \min(\epsilon_{IC,s}, \epsilon_{IC,max})$ , the condition for efficient TeV production is  $\epsilon_{IC,s} \geq 10^6$  and  $\epsilon_{IC,max} \geq 10^6$ . Since  $\epsilon_{IC,s} \sim \gamma_s b_s \gamma_{KN}$ , where  $\gamma_{KN} = 1/(4\epsilon_0) \sim 10^4$ , this translates into the condition  $b_s > 100$ , i.e., for a mono-energetic field, we again need a very large  $q \gtrsim 10^3$ . In the shocked wind scenario, this condition provides an upper limit on the strength of the magnetic field in the shocked plasma. In the bulk-Compton scenario, the condition is satisfied even for strongly magnetized winds. This is because electrons are cold and frozen to the magnetic field lines, hence their energy losses via the synchrotron mechanism are negligible and, effectively, the value of  $q$  is infinite. Of course, to reach TeV energies in this scenario, the bulk Lorentz factor of the wind is required to be of the order  $10^6$ , which is consistent with estimations of the wind speed in the Crab Nebula (Rees & Gunn 1974).

### 6.4. Kiloparsec scale jets

Jets in quasars encounter a variety of radiation fields as they make their way out from the central black hole, starting from the radiation field of the black hole accretion disk and ending with the cosmic microwave background (CMB). For jets that are relativistic from the start, the largest  $q$  would be reached near the base of the jet. The lack of bulk Compton features in the soft X-ray band suggests this is not the case (Moderski et al. 2004), and thus that the energetically dominant Compton interactions of a jet with external radiation field seem to take place not earlier than in the BEL region, i.e. around 0.1 – 1 parsec from the center. Large values of  $q$  are also expected in sources triggered at 1-10 parsec distances where the diffuse component of the external field is likely dominated by the thermal emission from hot dust (Sikora et al. 2002). At progressively larger distances, the jet undergoes Compton interactions with narrow emission lines, with stellar radiation, and finally the CMB. As of now there is no direct evidence that at such distances electrons are injected with  $b_{max} \gg 1$ , but this may simply be due to the sensitivity and angular resolution of present  $\gamma$ -ray detectors. Indirect evidence in favor of  $b_{max} \gg 1$  and  $q \gg 1$  for kiloparsec

scale jets may come from the work of Dermer and Atoyan (2002). They argued that a purely synchrotron emission model, with a jet magnetic energy density less than the CMB energy density, can successfully explain not just the observed radio-to-optical jet radiation, but also the X-ray flux detected by Chandra, despite the fact that the Chandra flux often lies above an extrapolation of the radio-optical spectrum. This is achieved by the formation of a synchrotron bump above  $\epsilon_{syn,KN}$  due to the KN effects we have described here. We note, however, this particular model requires extremely large  $\gamma_{max}$ , at least one order of magnitude larger than  $\gamma_{KN} = 1/(4\Gamma\epsilon_{CMB}) \simeq 2 \times 10^7/(\Gamma/10)(1+z)$ , where  $\epsilon_{CMB}(z=0) \sim 10^{-9}$ .

## 7. CONCLUSIONS

We have studied, both analytically and using accurate numerical codes, the electromagnetic spectra produced by relativistic electrons in a magnetized non-thermal source that is immersed in a dense radiation field originating outside the source. We consider the case when the steady-state electron energy distribution is determined by the injection energy spectrum of the accelerated electrons and their energy losses, dominated by synchrotron radiation and Compton scattering which may extend deeply into the KN regime. We concentrate on the poorly studied region of parameter space in which the energy density of the radiation field inside the source exceeds that of the magnetic field, i.e., values of the parameter  $q = u_0/u_B > 1$ . Fig. 10 summarizes the three main regions we find for the overall parameter space for our problem:

- In zone I ( $q < 1$ ), the electron distribution is determined by synchrotron cooling and KN effects do not appear in the synchrotron spectrum. The Compton spectrum, however, shows a strong break at  $\epsilon_{IC,KN}$  due to the strong KN reduction in the Compton scattering rate that starts for electron energies  $\gamma > \gamma_{KN}$ . Assuming the maximum electron acceleration energy,  $\gamma_{max}$ , is sufficiently large that  $\epsilon_{IC,max} > \epsilon_{IC,KN}$ , the position of this break is *independent* of  $\gamma_{max}$ . In zone Ib ( $1 < q \lesssim 3$ ), we start to see a hardening of the electron distribution that is reflected in the synchrotron emission spectrum. The hardening occurs because Compton cooling is now an important contribution to the total electron cooling rate, and Compton losses decrease at high energies due to the KN effect. The effect is not large, however. The Compton spectrum does not show significant differences because synchrotron losses start to dominate again at  $\gamma_s < \gamma_{KN}$ .
- In zones II and III,  $q \gg 1$ , and the distortion in the electron distribution due to the reduction in Compton cooling is very large. The synchrotron spectrum correspondingly shows a strong, hard excess over the Thomson limit asymptote. The Compton spectrum below  $\epsilon_{IC,s}$ , however, does not show a strong deviation from the low energy Thomson limit

because the KN decline in the Compton rate is compensated by the corresponding increase in the electron density. The distinction between zone II and III is that in zone II, the maximum electron energy is such that  $\gamma_{max} > \gamma_s$ . Above  $\gamma_s$ , synchrotron cooling dominates. The energy distributions of the electrons and the synchrotron radiation reach asymptotes with the same slopes as in the Thomson regime but with amplitudes enhanced by a factor  $q$ . The Compton spectrum, on the other hand, shows a strong break at  $\epsilon_{IC,s}$  because the KN reduction in the scattering is no longer compensated by a hardening of the electron energy distribution. In zone II, then, the Compton spectrum breaks at an energy *independent* of  $\gamma_{max}$ . In zone III, instead, the synchrotron losses never dominate, and the location of Compton high energy break is determined by the maximum electron energy just as it is for the synchrotron component. The combination of the high energy break and the hardening of the synchrotron spectrum at lower energies leads to the formation of a strong synchrotron bump.

The specific conclusions of our study are:

- The IC spectra have high energy breaks at  $\epsilon_{IC,max}$ , if  $b_{max} < b_s$ , or at  $\epsilon_{IC,s}$ , if  $b_{max} > b_s$ . The former is related to the high energy cut-off of electron injection function, the latter to the strong steepening of the IC spectrum, caused by domination of energy losses of electrons with  $\gamma > \gamma_s$  by synchrotron mechanism;
- Synchrotron spectra undergo strong hardening at  $\epsilon > \epsilon_{syn,KN}$ , with  $|\Delta\alpha|$  reaching  $\sim 0.5 - .75$  for  $q > 30$ . Hence, for very hard electron injection spectra, with  $p < 1$ , the spectral index  $\alpha$  ( $= 0.5 - |\Delta\alpha|$ ) can even reach negative values. The hardening is visible already at  $\epsilon \simeq 0.1\epsilon_{syn,KN}$ ;
- For  $1 < b_{max} \leq b_s$ , the hardening of the synchrotron spectrum combined with the high energy break at  $\epsilon_{s,max}$  leads to the formation a “bump” in the high-energy portion of the synchrotron spectrum. For  $b_{max} \gg b_s$ , the hardening of the synchrotron spectrum stops at  $\epsilon_{syn,s}$  and the spectrum continues with the same slope as in the Thomson regime but with a normalization  $q$  times larger;
- For hard electron injection functions ( $p < 2$ ) and  $b_{max} > b_s$ , the luminosity of the synchrotron component is larger than luminosity of the IC component, even for  $q \gg 1$ . This is because for a hard injection function most of the power is supplied to electrons with  $\gamma > \gamma_s$ , and the energy losses for these electrons are dominated by synchrotron radiation. For  $p = 2$ , the luminosities of the synchrotron and IC spectral peaks are of the same order;
- When KN effects are important, both the IC and especially the synchrotron component can have spectra *harder* than the hardest spectrum possible in the Thomson limit for fast cooling electrons ( $\alpha = 0.5$ );

- Generically, photon-photon pair production of the Compton gamma-rays on the ambient radiation field may be important for  $\gamma_{max} \gg \gamma_{KN}$ . However, for a pair production energy threshold exceeding  $\epsilon_{IC,s}$ , the fraction of the  $\gamma$ -ray luminosity converted into pairs is not significant, even if the opacity for pair production is large;
- The continuous energy loss approximation for the evolution of the electron distribution appears to work reasonably well, even for  $\gamma_{max} \gg \gamma_{KN}$ . Use of this approximation can save considerable computing time;
- The KN effects we have discussed can be important in powerful blazars and HMXB, with the latter including accreting compact objects and rotationally powered pulsars.

This project was partially supported by Polish KBN grants 1 P03D 00928, PBZ-KBN-054/P03/2001. M.S. and P.C. thank the Fellows of the MPI für Kernphysik, and SLAC and KIPAC for their hospitality and support during their stays there. P.C. was also supported in part by a Yale University Senior Faculty Fellowship.

## A. APPENDIX

### A.1. Scattering of directed photon beams on isotropically distributed relativistic electrons

The general formula for the distribution in energy and angle of the scattered photons per electron per unit time for the photon beams is given by Eq. (14) in Aharonian & Atoyan (1981). For  $\epsilon \gg \epsilon_0$  and  $\gamma \gg 1$ , this formula takes the form (see Eqs.[20] and [21] in Aharonian & Atoyan 1981)

$$\frac{\partial \dot{N}_{sc}(\epsilon, \gamma, \theta)}{\partial \epsilon \partial \Omega} \simeq \frac{3}{16\pi} c \sigma_T \int_{\epsilon_{0,m}(\gamma, \theta)} \frac{n_{\epsilon_0}}{\epsilon_0 \gamma^2} f(\epsilon, \epsilon_0, \gamma, \theta) d\epsilon_0, \quad (\text{A1})$$

where  $\epsilon_0$  and  $\epsilon$  are energies of the incident and scattered photons in  $m_e c^2$  units, respectively,  $\theta$  is the scattering angle,  $n_{\epsilon_0}$  is the photon number density per energy,

$$\epsilon_{0,m}(\gamma, \theta) = \frac{\epsilon}{2(1 - \cos \theta) \gamma^2 (1 - (\epsilon/\gamma))}, \quad (\text{A2})$$

and

$$f(\epsilon, \epsilon_0, \gamma, \theta) = 1 + \frac{w^2}{2(1-w)} - \frac{2w}{b_\theta(1-w)} + \frac{2w^2}{b_\theta^2(1-w)^2} \quad (\text{A3})$$

where  $b_\theta = 2(1 - \cos \theta) \epsilon_0 \gamma$ , and  $w = \epsilon/\gamma$ .

## A.2. Scattering of isotropically distributed photons on isotropically distributed relativistic electrons

For an isotropic radiation field

$$\frac{\partial \dot{N}_{sc}(\epsilon, \gamma)}{\partial \epsilon \partial \Omega} = \frac{1}{4\pi} \frac{\partial \dot{N}_{sc}(\epsilon, \gamma)}{\partial \epsilon} = \frac{3}{16\pi} c\sigma_T \int_{\epsilon_{0,m}(\gamma)} \frac{n_{\epsilon_0}}{\epsilon_0 \gamma^2} f_{iso}(\epsilon, \epsilon_0, \gamma) d\epsilon_0, \quad (\text{A4})$$

where (see Eq.[23] in Aharonian & Atoyan 1981)

$$\epsilon_{0,m}(\gamma) = \frac{\epsilon}{4\gamma^2(1 - (\epsilon/\gamma))}, \quad (\text{A5})$$

and

$$f_{iso}(\epsilon, \epsilon_0, \gamma) = \frac{1}{4\pi} \int_{\theta_{min}} f(\epsilon, \epsilon_0, \gamma, \theta) d\Omega = \frac{1}{2} \int^{\cos \theta_{min}} f(\epsilon, \epsilon_0, \gamma, \theta) d \cos \theta, \quad (\text{A6})$$

where  $\cos \theta_{min} = 1 - 2w/(b(1-w))$ . Integration in Eq. (A6) can be performed analytically giving (see Eq.[22] in Aharonian & Atoyan 1981)

$$f_{iso}(\epsilon, \epsilon_0, \gamma) = 1 + \frac{w^2}{2(1-w)} + \frac{w}{\tilde{b}(1-w)} - \frac{2w^2}{\tilde{b}^2(1-w)^2} - \frac{w^3}{2\tilde{b}(1-w)^2} - \frac{2w}{\tilde{b}(1-w)} \ln \frac{\tilde{b}(1-w)}{w}, \quad (\text{A7})$$

where  $\tilde{b} = 4\epsilon_0\gamma$  (note that  $f_{iso}$  is fully equivalent to the term bracketed in Eq.[9] in Jones [1968]).

## A.3. Electron energy losses

The rate of inverse-Compton energy losses of electrons is

$$|\dot{\gamma}|_{IC} \simeq \frac{3}{4} c\sigma_T \frac{1}{\gamma^2} \int \frac{n_{\epsilon_0}}{\epsilon_0} \left[ \int f_{iso}(\epsilon, \epsilon_0, \gamma) \epsilon d\epsilon \right] d\epsilon_0. \quad (\text{A8})$$

The inner integral has an analytical solution (see Eq. [46] in Jones 1968)

$$\int f_{iso}(\epsilon, \epsilon_0, \gamma) \epsilon d\epsilon = \frac{\gamma^2 g(\tilde{b})}{\tilde{b}} \quad (\text{A9})$$

where

$$g(\tilde{b}) = \left( \frac{1}{2}\tilde{b} + 6 + \frac{6}{\tilde{b}} \right) \ln(1 + \tilde{b}) - \left( \frac{11}{12}\tilde{b}^3 + 6\tilde{b}^2 + 9\tilde{b} + 4 \right) \frac{1}{(1 + \tilde{b})^2} - 2 + 2\text{Li}_2(-\tilde{b}). \quad (\text{A10})$$

and  $\text{Li}_2$  is the dilogarithm. Hence,

$$|\dot{\gamma}|_{IC} = \frac{4c\sigma_T}{3} \gamma^2 \int f_{KN}(\tilde{b}) \epsilon_0 n_{\epsilon_0} d\epsilon_0 \quad (\text{A11})$$

where

$$f_{KN}(\tilde{b}) = 9g(\tilde{b})/\tilde{b}^3. \quad (\text{A12})$$



## REFERENCES

- Aharonian, F.A., & Atoyan, A.M. 1981, *Astrophys. & Space Sci.* 79, 321
- Aharonian, F.A. et al. 2005, *A&A*, submitted.
- Ball, L., & Kirk, J.G. 2000, *Astropart. Phys.*, 12, 335
- Blumenthal, G.R., & Gould, R.J. 1970, *Rev. Mod. Phys.*, 42, 237
- Błażejowski, M., Sikora, M., Moderski, R., & Madejski, G. 2000, *ApJ*, 545, 107
- Combi, J.A., Ribó, M., Mirabel, I.F., & Sugizaki, M. 2004, *A&A*, 422, 1031
- Coppi, P.S. 1992, *MNRAS*, 258, 657
- Coppi, P.S. & Blandford, R.D. 1990, *MNRAS*, 245, 453
- Coppi, P.S. & Aharonian, F.A. 1999, *Aph*, 11, 35.
- Dermer, C.D., & Atoyan, A.M. 2002, *ApJ*, 568, L81
- Fender, R., & Belloni, T. 2004, *ARAA*, 42, 317
- Georganopoulos, M., Aharonian, F.A., & Kirk, J.G. 2002, *A&A*, 388, L25
- Johnston, S., Manchester, A.G., Lyne, M. et al. 1992, *ApJ*, 387, L37
- Jones, F.C. 1968, *Phys. Rev.*, 167, 1159
- Kaspi, V.M., Johnston, S., Bell, R.N., et al. 1994, *ApJ*, 423, L43
- Khangulian, D. & Aharonian, F.A., *AIP Conf. Proc.* 745, 359.
- Kirk, J.G., Rieger, F.M., & Mastichiadis, A. 1998, *A&A*, 333, 452
- Kusunose, M., & Takahara, F. 2005, *ApJ*, 621, 285
- Kusunose, M., Takahara, F., & Kato, T. 2004, *Progress of Theoretical Physics Supplement*, 155, 367
- Massi, M., Ribó, M., Paredes, J.M., et al. 2004, *A&A*, 414, L1
- Moderski, R., Sikora, M., Madejski, G.M., & Kamae, T. 2004, *ApJ*, 611, 770
- von Montigny, C., Bertsch, D.L., Chiang, J., et al. 1995, *ApJ*, 440, 525

- Mukherjee, R., Bertsch, D.L., Bloom, S.D., et al. 1997, *ApJ*, 490, 116
- Padovani, P., Costamante, L., Ghisellini, G., et al. 2002, *ApJ*, 581, 895
- Padovani, P., Perlman, E.S., Landt, H., et al. 2003, *ApJ*, 588, 128
- Paredes, J.M., Martí, J., Ribó, M., & Massi, M. 2000, *Science*, 288, 2340
- Ravasio, M., Tagliaferri, G., Ghisellini, G., et al. 2003, *A&A*, 408, 479
- Rees, M.J., & Gunn, J.E. 1974, *MNRAS*, 167, 1
- Sikora, M., Begelman, M.C., & Rees, M.J. 1994, *ApJ*, 421, 153
- Sikora, M., Błażejowski, M., Moderski, R., & Madejski, G.M. 2002, *ApJ*, 577, 78
- Tavecchio, F., Maraschi, L., & Ghisellini, G. 1998, *ApJ*, 509, 608
- Zdziarski, A.A. 1988, *ApJ*, 335, 786
- Zdziarski, A.A. 1989, *ApJ*, 342, 1108
- Zdziarski, A.A., & Krolik, J.H. 1993, *ApJ*, 409, L33

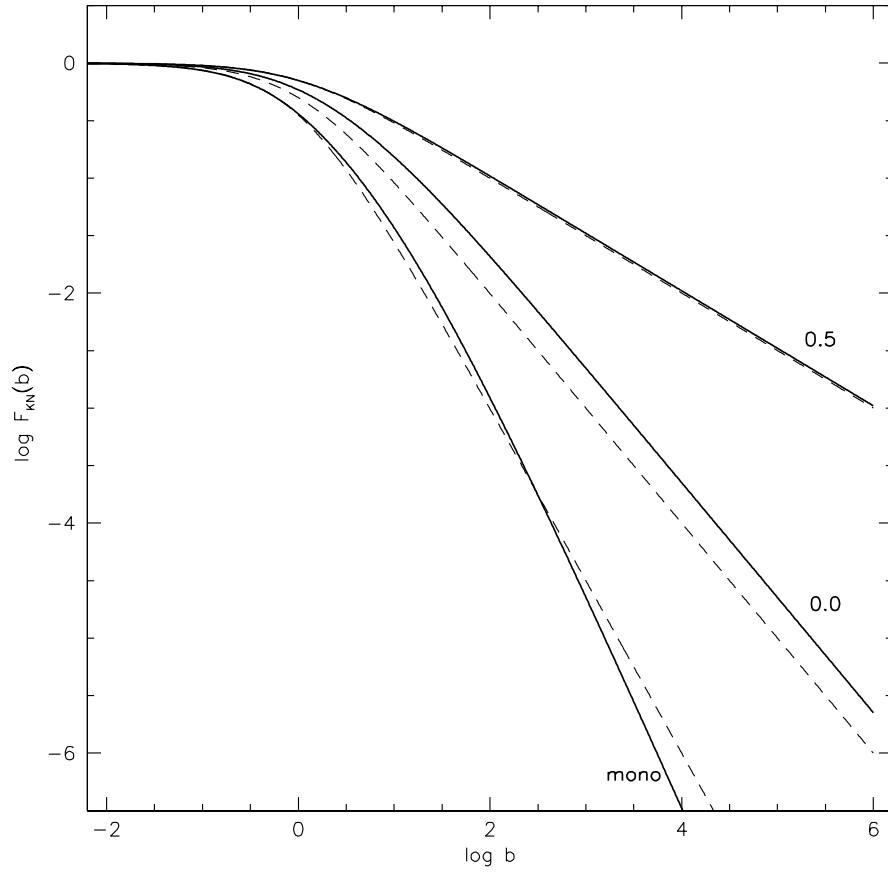


Fig. 1.— The function  $F_{KN}(b)$  computed for mono-energetic (“mono”) and power law ( $\alpha_0 = 0.0$  and  $\alpha_0 = 0.5$ ) energy distributions of the external photon field. The solid lines show the results of the exact calculations while the dashed lines are the analytical approximations.

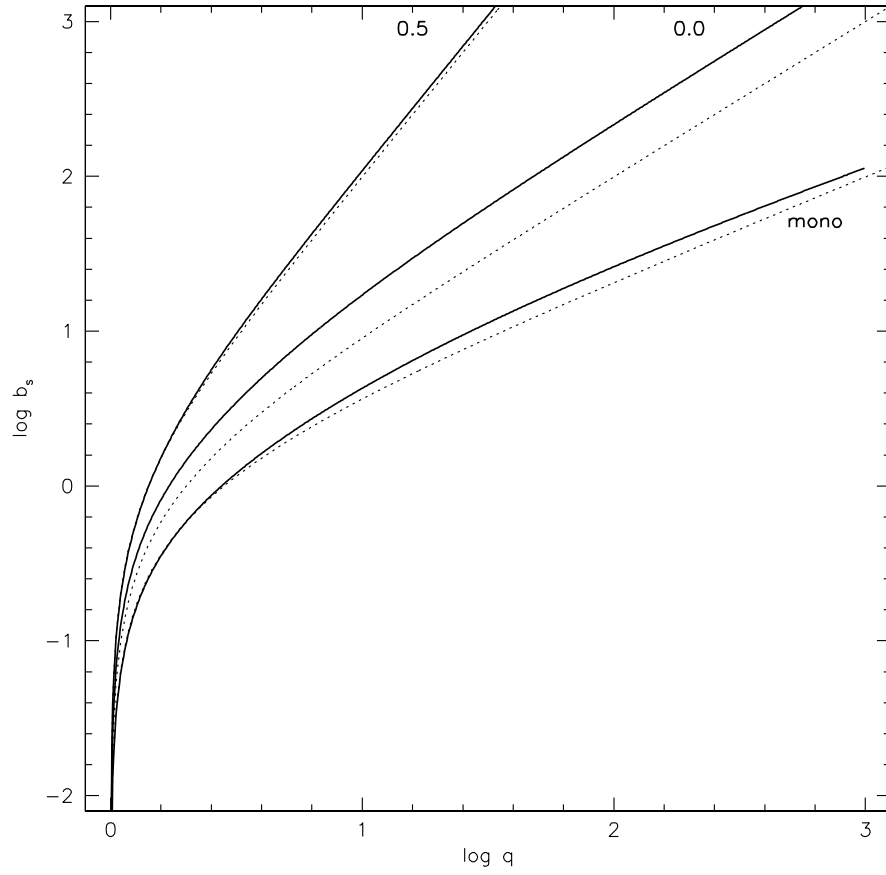


Fig. 2.—  $b_s$  vs  $q$  for: mono-energetic and power law ambient radiation fields. Solid lines – exact results, dashed lines – analytical approximations.

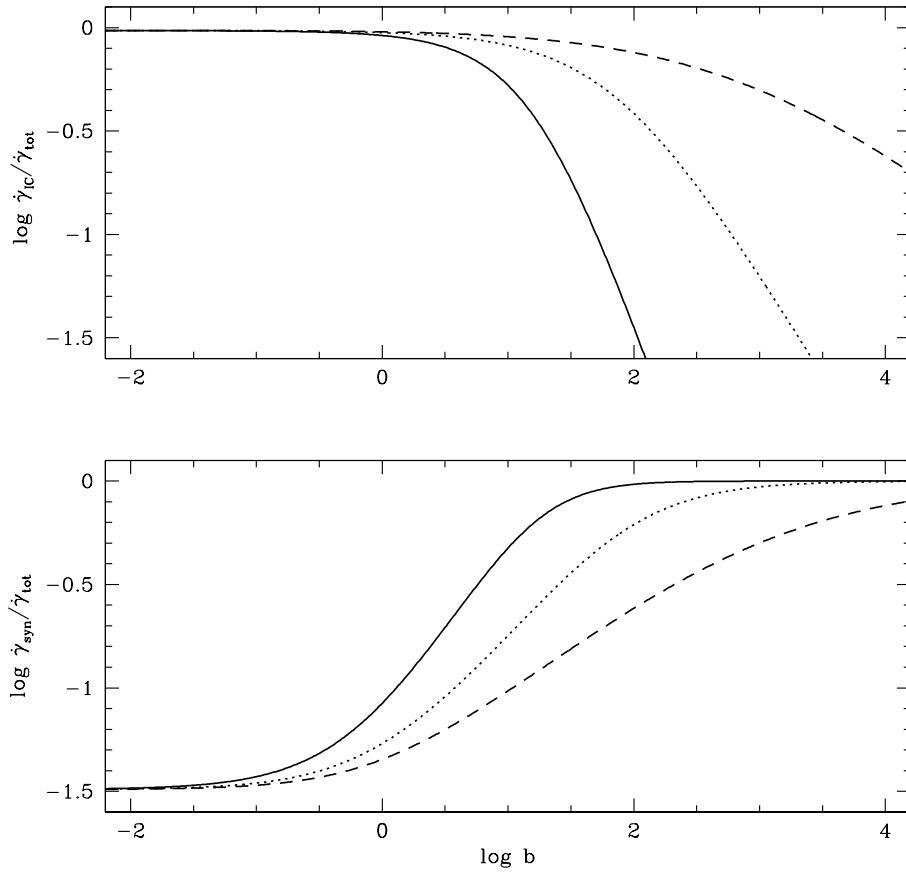


Fig. 3.— The relative IC and synchrotron energy losses for an ambient radiation energy distribution that is mono-energetic (solid lines) or power law ( $\alpha_0 = 0.0$  – dotted lines;  $\alpha_0 = 0.5$  – dashed lines).

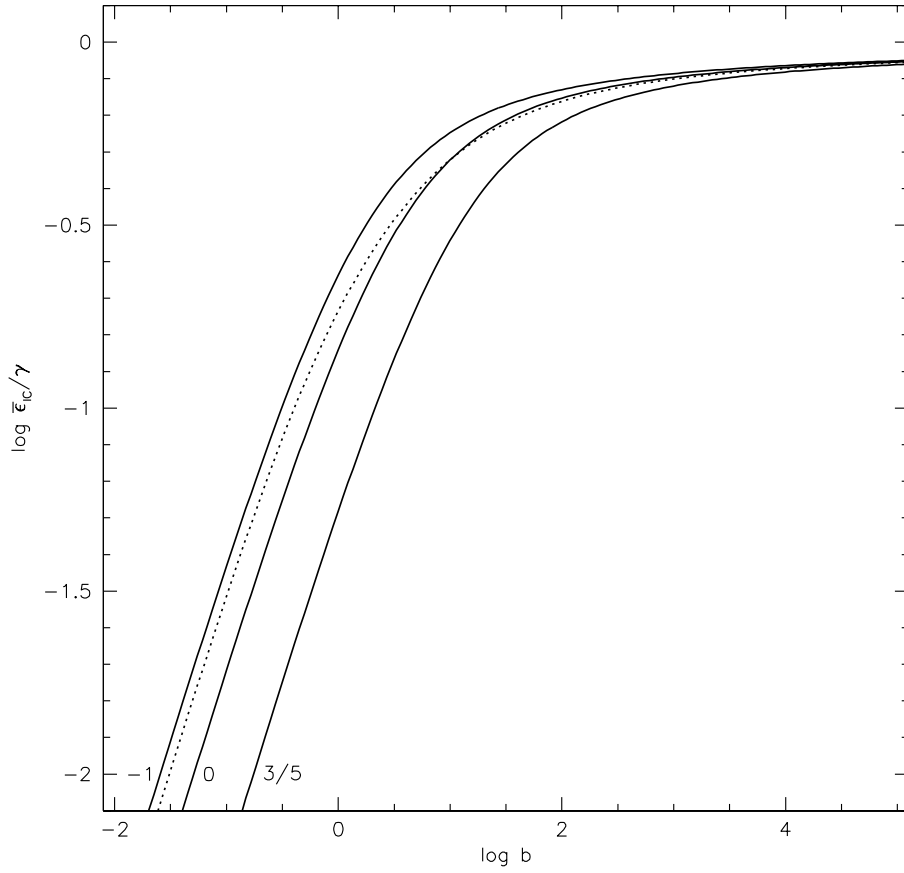


Fig. 4.— Inelasticity,  $\mathcal{A} = \bar{\epsilon}_{IC}(\gamma)/\gamma$  for electron Compton scatterings off a mono-energetic ambient radiation field. Dotted line – isotropic ambient radiation field. Solid lines – beamed ambient radiation field, for scattering angles  $\cos \theta = -1.0, 0.0,$  and  $0.6$ .

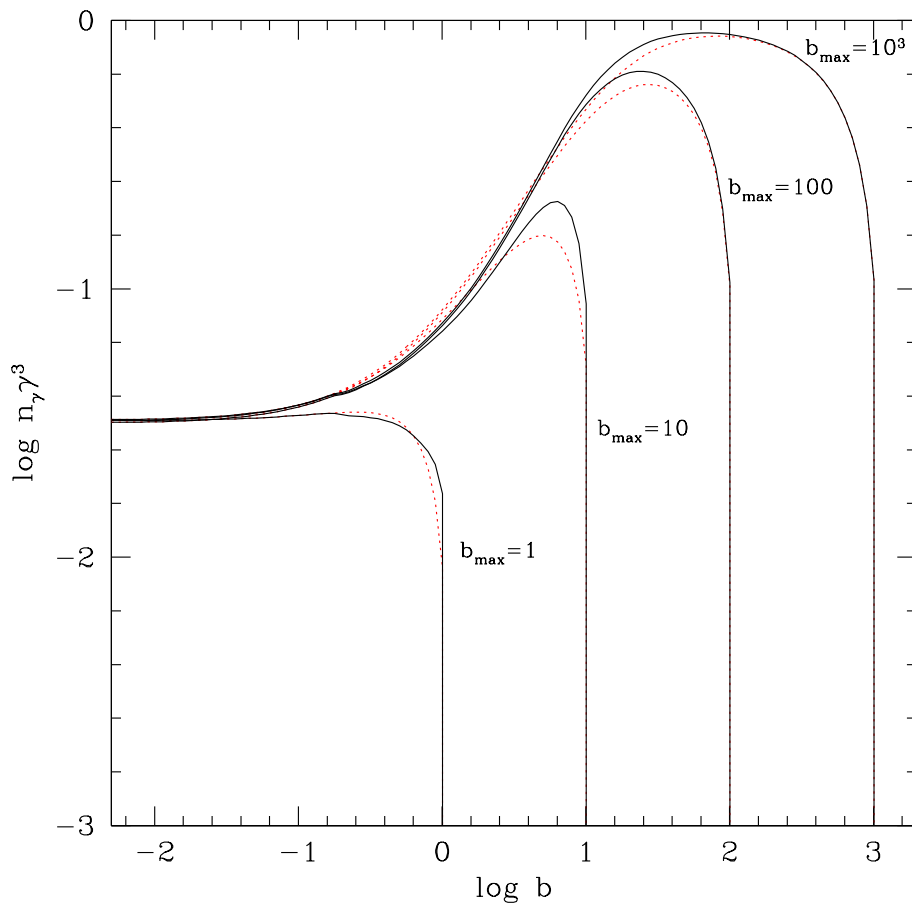


Fig. 5.— Steady state electron energy distributions for power-law electron injection function,  $Q \propto \gamma^{-p}$ , and mono-energetic ambient radiation field. Solid lines – exact results; dotted lines – results obtained using the continuous energy loss approximation for all Compton scattering. The model parameters are:  $p = 2$ ,  $q = 30$ ;  $b_{max} = 1; 10; 10^2; 10^3$ .

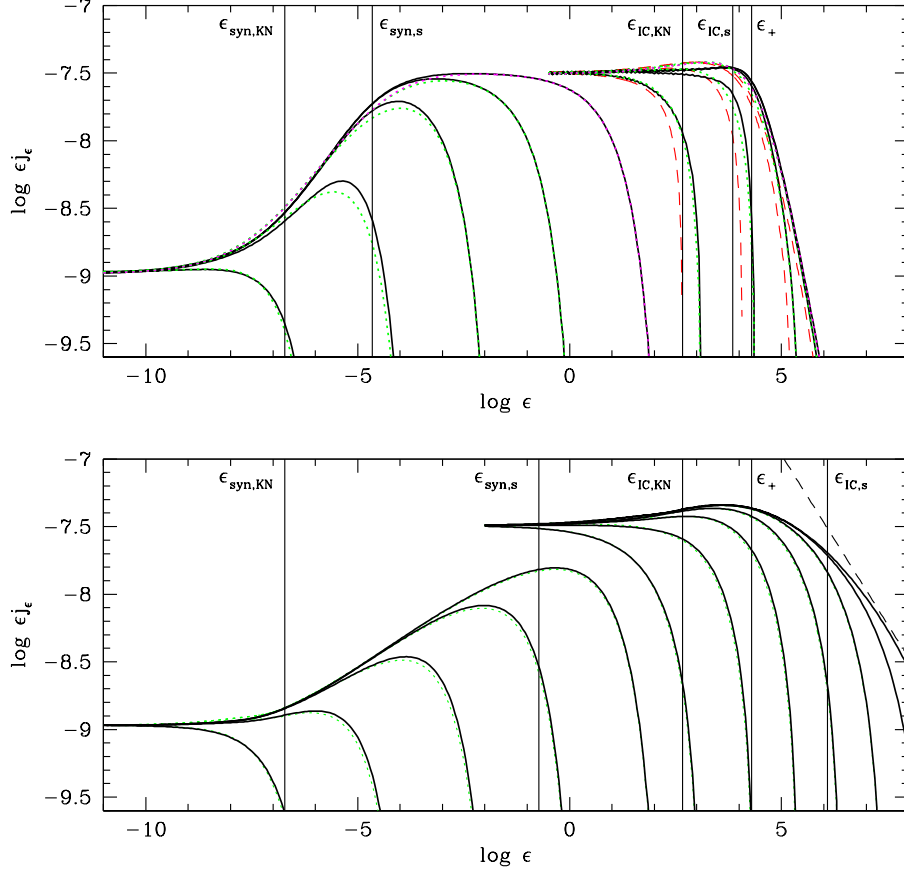


Fig. 6.— Inverse-Compton plus synchrotron spectra of steady sources. with model parameters  $p = 2$ ;  $q = 30$ ;  $b_{max} = 1, 10, 10^2, 10^3, 10^4$ ;  $\epsilon_0 = 10^{-4}$ ;  $B = 1\text{Gauss}$ . (a) Upper panel – mono-energetic ambient radiation field. (b) Lower panel – power-law ambient radiation field with  $\alpha_0 = 0.5$ . Solid lines – exact calculations. Dotted lines – calculations using continuous energy loss approximation. Dashed lines – Compton spectra computed using the continuous energy loss approximation and the delta-function approximation. The dot-dashed line in the lower panel is the asymptotic power law ( $\alpha = -0.5$ ) for the IC spectrum at  $\epsilon > \epsilon_{IC,s}$  given by Eq. (31). To show convergence to this spectrum for increasing  $b_{max}$ , the lower panel also shows the IC spectra obtained for  $b_{max} = 10^5, 10^6$ , and  $10^7$ .



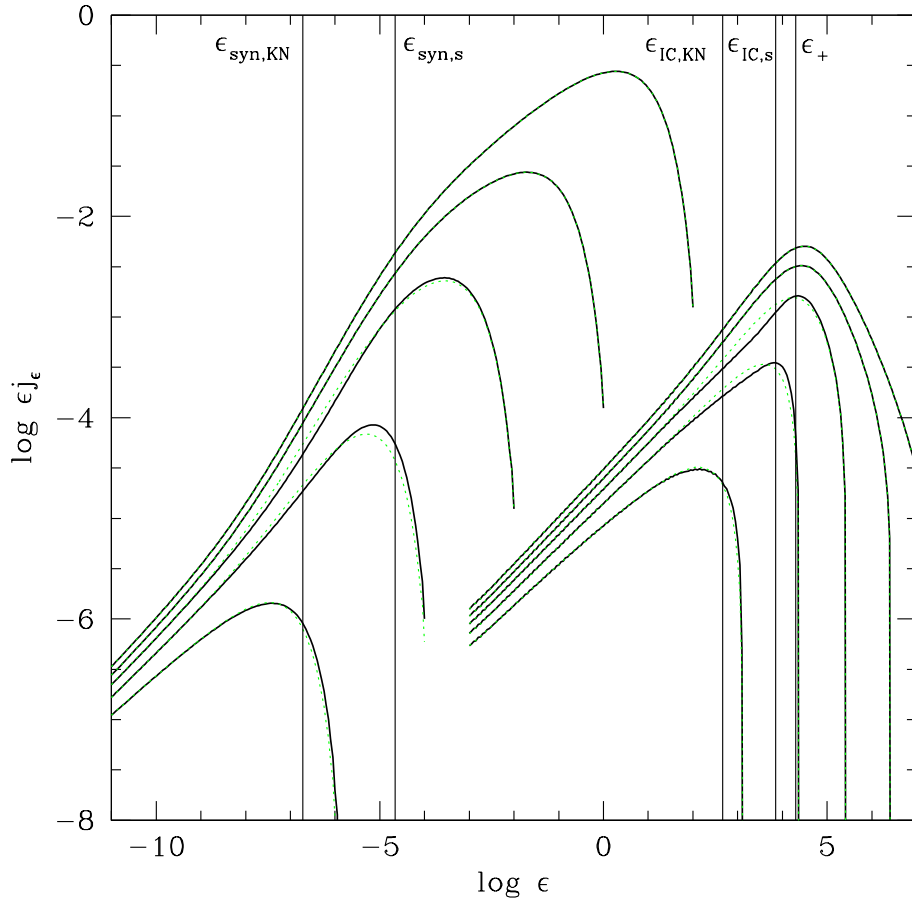


Fig. 7.— Same as the upper panel of Fig. 6 (mono-energetic radiation field), but for  $p = 1$ .

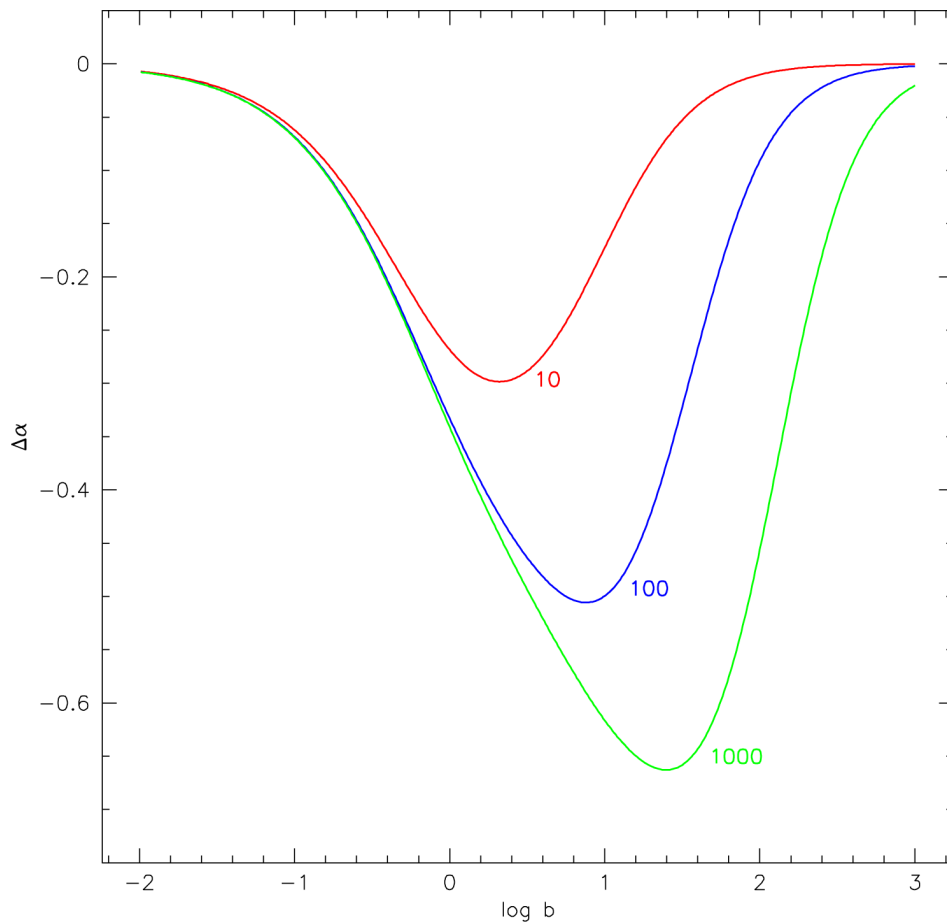


Fig. 8.— Synchrotron spectral 'hardening',  $\Delta\alpha$ , as a function of  $b$ . Model parameters:  $b_{max} = \infty$ , and  $q = 10, 10^2, 10^3$ .

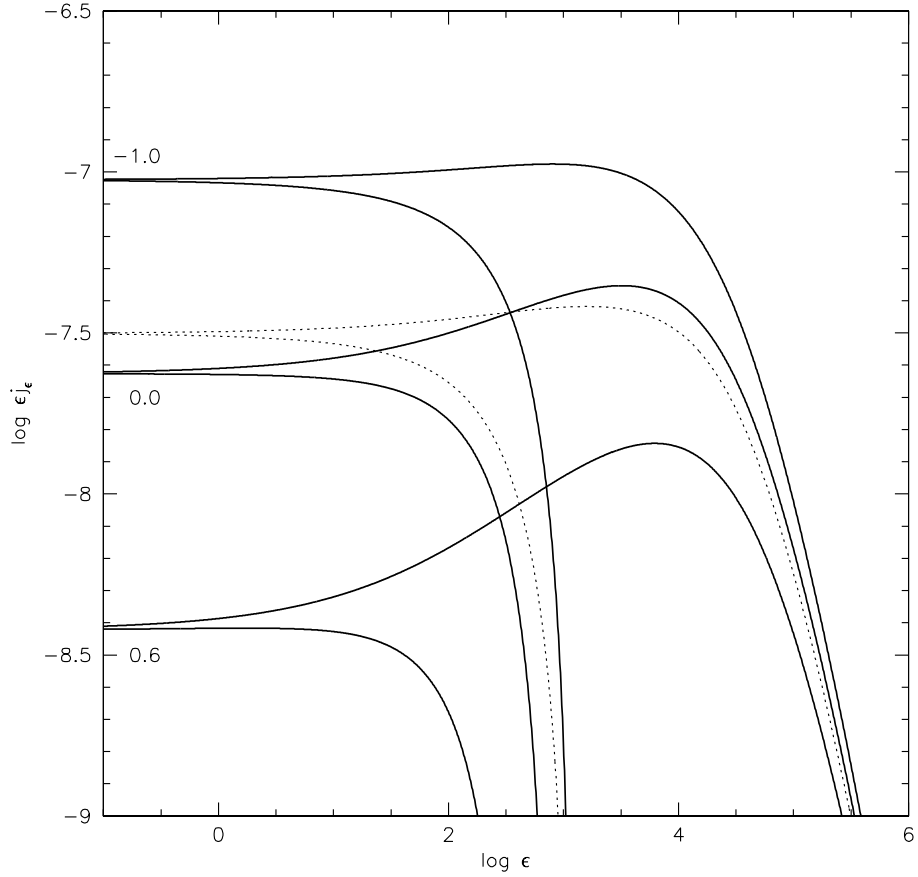


Fig. 9.— Inverse-Compton spectra for a beamed ambient radiation field. The model parameters:  $q = 30$ ,  $b_{max} = 10, 10^3$ ;  $\epsilon_0 = 10^{-4}$ ;  $\cos \theta = -1.0, 0.0, 0.6$ . For comparison, the IC spectra for an isotropic ambient radiation field are also shown (dotted lines).

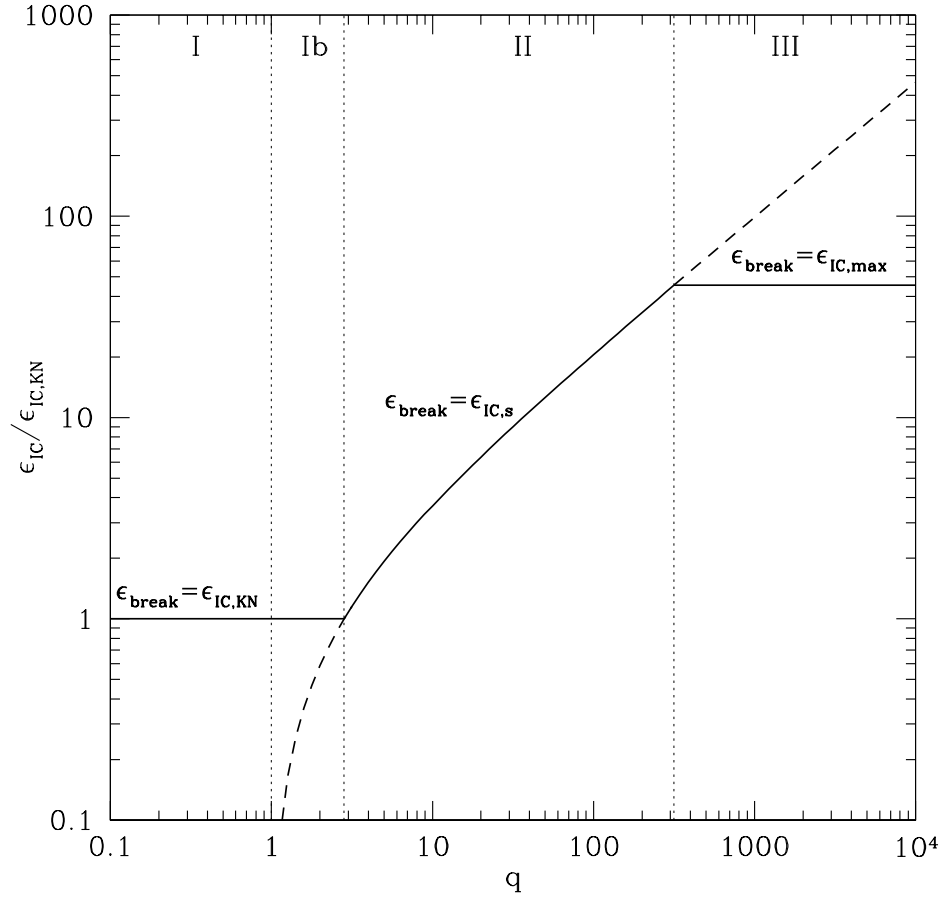


Fig. 10.— Schematic illustration showing the location of the high-energy break in the Compton spectra as a function of  $q$ . (For details, see text.)